Timescales for radiation belt electron acceleration and loss due to resonant wave-particle interactions: 2. Evaluation for VLF chorus, ELF hiss, and electromagnetic ion cyclotron waves

Danny Summers,[1] Binbin Ni,[1] and Nigel P. Meredith[2]

Received 28 July 2006; revised 9 November 2006; accepted 22 November 2006; published 13 April 2007.

[1] Outer zone radiation belt electrons can undergo gyroresonant interaction with various magnetospheric wave modes including whistler-mode chorus outside the plasmasphere and both whistler-mode hiss and electromagnetic ion cyclotron (EMIC) waves inside the plasmasphere. To evaluate timescales for electron momentum diffusion and pitch angle diffusion, we utilize bounce-averaged quasi-linear diffusion coefficients for field-aligned waves with a Gaussian frequency spectrum in a dipole magnetic field. Timescales for momentum diffusion of MeV electrons due to VLF chorus can be less than a day in the outer radiation belt. Equatorial chorus waves ($|\lambda_W| < 15$ deg) can effectively accelerate MeV electrons. Efficiency of the chorus acceleration mechanism is increased if high-latitude waves ($|\lambda_W| > 15$ deg) are also present. Our calculations confirm that chorus diffusion is a viable mechanism for generating relativistic (MeV) electrons in the outer zone during the recovery phase of a storm or during periods of prolonged substorm activity when chorus amplitudes are enhanced. Radiation belt electrons are subject to precipitation loss to the atmosphere due to resonant pitch angle scattering by plasma waves. The electron precipitation loss timescale due to scattering by each of the wave modes, chorus, hiss, and EMIC waves, can be 1 day or less. These wave modes can separately, or in combination, contribute significantly to the depletion of relativistic (MeV) electrons from the outer zone over the course of a magnetic storm. Efficient pitch angle scattering by whistler-mode chorus or hiss typically requires high latitude waves ($|\lambda_W| > 30$ deg). Timescales for electron acceleration and loss generally depend on the spectral properties of the waves, as well as the background electron number density and magnetic field. Loss timescales due to EMIC wave scattering also depend on the ion (H^+, He^+, O^+) composition of the plasma. Complete models of radiation belt electron transport, acceleration and loss should include, in addition to radial (cross-L) diffusion, resonant diffusion due to gyroresonance with VLF chorus, plasmaspheric hiss, and EMIC waves. Comprehensive observational data on the spectral properties of these waves are required as a function of spatial location (L, MLT, MLAT) and magnetic activity.

Citation: Summers, D., B. Ni, and N. P. Meredith (2007), Timescales for radiation belt electron acceleration and loss due to resonant wave-particle interactions: 2. Evaluation for VLF chorus, ELF hiss, and electromagnetic ion cyclotron waves, *J. Geophys. Res.*, *112*, A04207, doi:10.1029/2006JA011993.

1. Introduction

[2] Despite more than 40 years of research in magnetospheric physics, the dynamics of the Earth's electron radiation belts are not well understood. Understanding the behavior of relativistic (MeV) electrons in the outer radiation belt ($3 < L < 7$) is of particular interest since relativistic electrons can cause serious damage to spacecraft [e.g., *Baker*, 2002]. Nowcasting and forecasting of relativistic electron fluxes in the inner magnetosphere are important facets of space weather science. Enhanced fluxes of relativistic electrons appear in the outer zone following some magnetic storms. Storms or relativistic electron events result from various forms of solar wind driver, including high-speed solar wind streams [*Baker et al.*, 1997; *Blake et al.*, 1997], coronal mass ejections [*Reeves et al.*, 1998; *Baker et al.*, 1998], and interplanetary shocks [*Li et al.*, 1993]. *Reeves et al.* [2003] examined a full solar cycle (1989–2000) of data, involving 276 magnetic storms, to quantify the relationship between storms and the changes in relativistic electron flux in the radiation belts. Remarkably, it was

[1]Department of Mathematics and Statistics, Memorial University of Newfoundland, St. John's, Newfoundland, Canada.
[2]British Antarctic Survey, Natural Environment Research Council, Cambridge, UK.

Copyright 2007 by the American Geophysical Union.
0148-0227/07/2006JA011993

found that only about a half of all storms increased the fluxes of relativistic electrons, one quarter decreased the fluxes, and one quarter produced negligible change in the fluxes. It is clear that storms do not simply energize the radiation belts. Relativistic electron fluxes following a storm result from a competition between processes of electron acceleration and loss [e.g., *Summers et al.*, 2004a; *Thorne et al.*, 2005a].

[3] Processes governing the transport, acceleration, and loss of radiation belt electrons are discussed by *Li et al.* [1997], *Summers and Ma* [2000], *Li and Temerin* [2001], *Friedel et al.* [2002], *O'Brien et al.* [2003], *Green and Kivelson* [2004], *Green et al.* [2005], and *Thorne et al.* [2005a]. The papers by *Gendrin* [2001], *Horne* [2002], and *Thorne et al.* [2005a] assess the influence of wave-particle interactions on radiation belt electron dynamics. *Schulz and Lanzerotti* [1974] established radial (cross-L) diffusion as a fundamental energization and transport mechanism in the radiation belts. Radial diffusion driven by enhanced ULF waves can generate relativistic electrons during storms [*Hudson et al.*, 2001; *Elkington et al.*, 2003], though this generation mechanism does not appear to be effective inside geosynchronous orbit. Since the early work of *Kennel and Petschek* [1966] on pitch angle scattering of radiation belt particles, it has been known that gyroresonant wave-particle interactions can play a crucial role in magnetospheric physics. In the present paper we now restrict our attention to cyclotron resonant interactions of radiation belt electrons with whistler-mode chorus, plasmaspheric hiss, and electromagnetic ion cyclotron (EMIC) waves. In the companion paper, *Summers et al.* [2007] present local pitch angle, mixed (pitch angle, momentum), and momentum diffusion rates ($D_{\alpha\alpha}$, $|D_{\alpha p}|/p$, D_{pp}/p^2) for cyclotron resonance with field-aligned waves with a Gaussian frequency spectrum in a hydrogen or multi-ion (H^+, He^+, O^+) plasma. *Summers et al.* [2007] further derive the corresponding bounce-averaged diffusion rates ($\langle D_{\alpha\alpha}\rangle$, $\langle|D_{\alpha p}|\rangle/p$, $\langle D_{pp}\rangle/p^2$), assuming a dipole geomagnetic field. Here we apply these bounce-averaged diffusion rates to determine timescales for the acceleration and loss of radiation belt electrons due to cyclotron resonance with the three aforementioned magnetospheric wave modes. We consider electron gyroresonant interaction with whistler-mode (VLF) chorus, plasmaspheric (ELF) hiss, and EMIC waves in sections 2, 3, and 4, respectively. By applying quasi-linear theory, we determine the average effects of gyroresonant diffusion and exclude such highly nonlinear effects as phase trapping by a wave field. In section 5 we determine electron loss timescales due to combined scattering by VLF chorus, ELF hiss, and EMIC waves. Finally, in section 6 we state our conclusions.

2. Interaction of Electrons With Whistler-Mode Chorus Waves

[4] Whistler-mode chorus emissions are observed outside the plasmasphere over a broad range of local times (2200–1300 MLT) with typical frequencies in the range 0.05–0.8 $|\Omega_e|$, where $|\Omega_e|$ is the electron gyrofrequency [*Tsurutani and Smith*, 1974, 1977; *Koons and Roeder*, 1990; *Meredith et al.*, 2001; *Santolik et al.*, 2003, 2004]. VLF chorus occurs in two frequency bands, a lower band (0.1–0.5 $|\Omega_e|$) and an upper band (0.5–1.0 $|\Omega_e|$) [*Burtis and Helliwell*, 1976; *Meredith et al.*, 2001]. Equatorial chorus ($|\lambda| < 15$ deg) can be excited by cyclotron resonance with anisotropic 10–100 keV electrons injected near midnight from the plasmasheet [*Kennel and Petschek*, 1966]. High-latitude chorus ($|\lambda| > 15$ deg) may be generated in the horns of the magnetosphere [*Meredith et al.*, 2001]. *Santolik et al.* [2005] find that equatorial chorus in the upper band extends to about $L = 8$, and in the lower band (below 0.4 $|\Omega_e|$) to $L = 11$–12. Typical chorus amplitudes are 1–100 pT [*Burtis and Helliwell*, 1975; *Meredith et al.*, 2003a], though amplitudes up to 1 nT have been reported during intense geomagnetic activity [*Parrot and Gaye*, 1994]. Chorus emissions are predominantly substorm dependent, and all chorus emissions intensify when substorm activity is enhanced [*Meredith et al.*, 2001].

[5] Relativistic electrons drift in approximately circular trajectories eastward about the Earth and intersect the spatial zone of chorus emissions for more than 50% of their orbit. Consequently, relativistic electrons are subject to energy diffusion and pitch angle scattering due to gyroresonance with chorus emissions in the lower-density region outside the plasmapause. *Summers et al.* [1998] constructed resonant diffusion curves and showed that electron gyroresonance with whistler-mode chorus provides a viable mechanism for generating relativistic electrons. Models using a test-particle approach [*Roth et al.*, 1999], the quasi-linear diffusion formalism [*Summers and Ma*, 2000; *Summers et al.*, 2002, 2004b; *Miyoshi et al.*, 2003; *Horne et al.*, 2005a, 2005b; *Varotsou et al.*, 2005; *Shprits et al.*, 2006a], and a self-consistent wave-particle simulation code [*Katoh and Omura*, 2004] confirm that electron acceleration by the chorus diffusion mechanism could explain the increase of relativistic electron flux observed during storms or periods of prolonged substorm activity. Various observational studies [e.g., *Meredith et al.*, 2002a, 2002b, 2003b; *Miyoshi et al.*, 2003; *Smith et al.*, 2004; *Iles et al.*, 2006] provide evidence for chorus-driven electron acceleration to relativistic energies in regions outside the plasmasphere during geomagnetically disturbed periods.

[6] Whistler-mode chorus can also cause significant pitch angle scattering of electrons into the loss cone leading to precipitation losses from the outer radiation belt [*Lorentzen et al.*, 2001; *O'Brien et al.*, 2004; *Summers et al.*, 2005; *Thorne et al.*, 2005b]. Microbursts of relativistic (MeV) electron precipitation observed on SAMPEX [*O'Brien et al.*, 2004] can be explained by first-order electron cyclotron resonance with whistler-mode chorus [*Thorne et al.*, 2005b].

[7] Whistler-mode chorus waves comprise repeated narrowband monochromatic signals with rising frequency [*Anderson and Kurth*, 1989; *Sazhin and Hayakawa*, 1992; *Santolik et al.*, 2003, 2004]. In this paper we average over a specified band of chorus emission and treat chorus waves as broadband and phase-incoherent. The quasi-linear diffusion theory described in *Summers et al.* [2007] can therefore be applied to treat chorus interactions with radiation belt electrons. We expect that quasi-linear theory can give a reasonable description of chorus/electron resonant diffusion, even though the quasi-linear formalism cannot take account of nonlinear effects such as trapping in momentum space. The studies by *Albert* [2002] and *Trakhtengerts et al.* [2003]

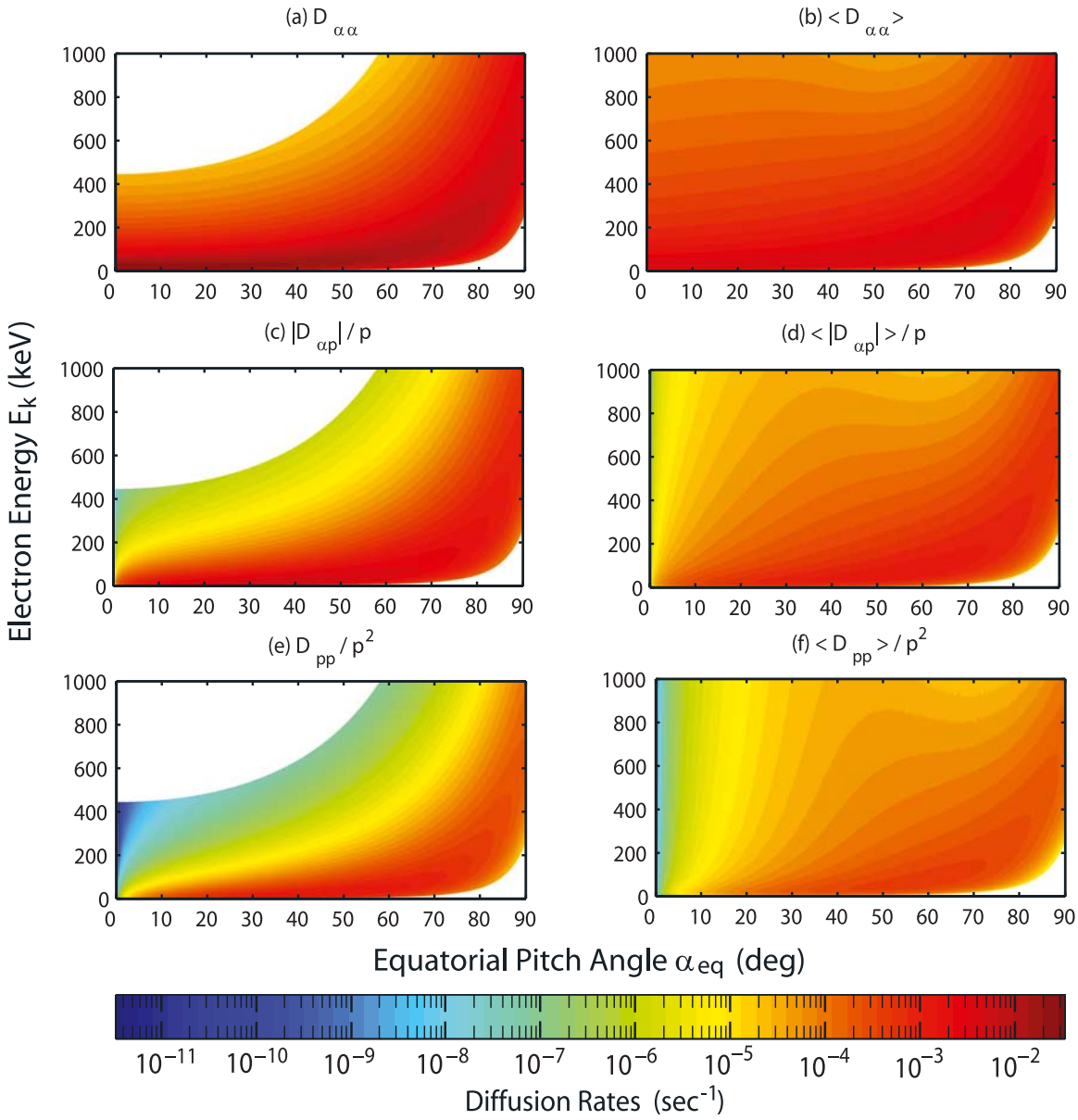

Figure 1. Two-dimensional plot of (left) local diffusion rates ($D_{\alpha\alpha}$, $|D_{\alpha p}|/p$, D_{pp}/p^2) and (right) corresponding bounce-averaged rates ($\langle D_{\alpha\alpha}\rangle$, $\langle|D_{\alpha p}|\rangle/p$, $\langle D_{pp}\rangle/p^2$) for electrons interacting with chorus, at $L = 4.5$, for $\alpha^* = \Omega_e^2/\omega_{pe}^2 = 0.16$, and wave amplitude $\Delta B = 0.1$ nT. Wave spectrum is Gaussian with $0.05\ |\Omega_e| < \omega < 0.65\ |\Omega_e|$ and $\omega_m = 0.35\ |\Omega_e|$, $\delta\omega = 0.15\ |\Omega_e|$.

show that electron acceleration due to phase trapping by a monochromatic wave can in fact exceed stochastic acceleration predicted by quasi-linear theory. By means of test particle simulations, *Omura and Summers* [2006] demonstrated that the energization of electrons trapped by a monochromatic VLF wave is considerably enhanced in the case of increasing wave frequency (corresponding to a rising tone) compared to the case of constant frequency.

[8] In the present study we base our calculations on the assumption that chorus waves are field-aligned. This simplifying assumption is partly justified by the studies of *Summers* [2005] and *Thorne et al.* [2005b] who found that first-order cyclotron resonant scattering rates of electrons by whistler-mode chorus agree very well with rates calculated assuming a wide-angle spectrum and ±5 harmonic resonances. Further, *Shprits et al.* [2006b] compared bounce-averaged diffusion rates for field-aligned and oblique waves and found that errors associated with the neglect of higher-order resonances are smaller than inaccuracies associated with uncertainties in the input values for the plasma density and latitudinal distribution of the waves.

[9] We now calculate diffusion rates for electrons interacting with whistler-mode chorus outside the plasmasphere. In Figures 1–7 we adopt the wave properties as used in Figures 1–2 of *Summers* [2005]. We assume a Gaussian frequency spectrum, equation (2) in the work of *Summers et al.* [2007], with $\omega_1 = 0.05\ |\Omega_e|$ as the lower frequency limit, $\omega_2 = 0.65\ |\Omega_e|$ as the upper frequency limit, $\omega_m = 0.35\ |\Omega_e|$ as the frequency of maximum wave power, $\delta\omega = 0.15\ |\Omega_e|$, and we set the wave amplitude $\Delta B = 0.1$ nT. The parameter

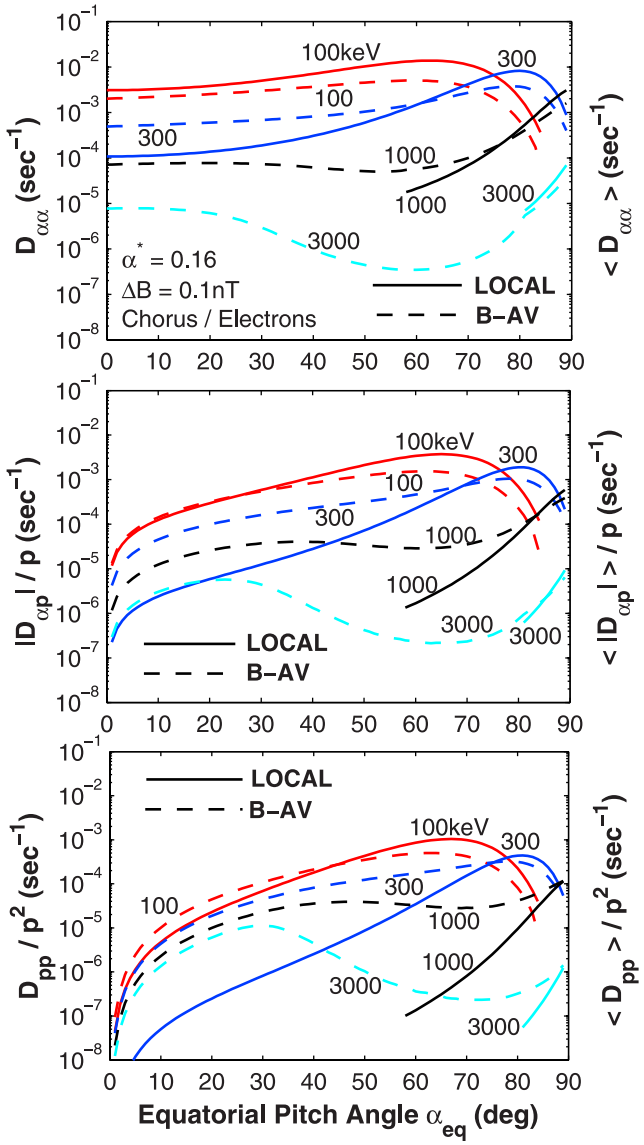

Figure 2. Local and bounce-averaged diffusion rates for electrons interacting with chorus, at $L = 4.5$, for the specified energies. Wave spectrum is as adopted in Figure 1.

$\alpha^* = \Omega_e^2/\omega_{pe}^2$, where ω_{pe} is the electron plasma frequency, plays an important role in cold plasma theory. In Figures 1 and 2 we focus our attention on the center of the outer radiation belt and we put $L = 4.5$, and take $\alpha^* = 0.16$ which corresponds to the electron number density $N_0 = 7.1$ cm^{-3}, typical of the equatorial region outside the plasmasphere [*Meredith et al.*, 2003a]. We further assume in Figures 1 and 2 that the chorus waves are distributed latitudinally along the entire magnetic field line. Figure 1 comprises two-dimensional plots of electron diffusion rates in (equatorial pitch angle, energy) space over the range ($0 \le \alpha_{eq} \le 90$ deg, $E_k \le 1$ MeV). Local pitch angle, mixed (pitch angle, momentum), and momentum diffusion rates ($D_{\alpha\alpha}$, $|D_{\alpha p}|/p$, D_{pp}/p^2) are shown on the left, with the corresponding bounce-averaged rates ($\langle D_{\alpha\alpha}\rangle$, $\langle|D_{\alpha p}|\rangle/p$, $\langle D_{pp}\rangle/p^2$) on the right. Diffusion coefficients are zero in the blank regions of the graphs (see section 3 of *Summers et al.* [2007] for details on the calculation of (E_k, α) resonance regions). Corresponding to the wave conditions in Figure 1, we plot in Figure 2 local and bounce-averaged electron diffusion rates at particular energies, as specified. Figures 1 and 2 demonstrate that the values of both local and bounce-averaged diffusion coefficients are sensitively dependent on pitch angle and energy. Moreover, these figures show that the overall effects of bounce-averaging are likewise dependent on pitch angle and energy. A general effect of bounce-averaging is to extend the region of (energy, pitch angle) space over which resonance takes place. This is due to the off-equatorial resonances that are accounted for by the bounce-averaging process. In Figures 1a and 1b and Figure 2 (top) we see that for MeV electrons bounce-averaging extends the range of pitch angle scattering into the loss cone. Pitch-angle scattering of higher-energy electrons ($E_k > 300$ keV) is more efficient at higher latitudes than at

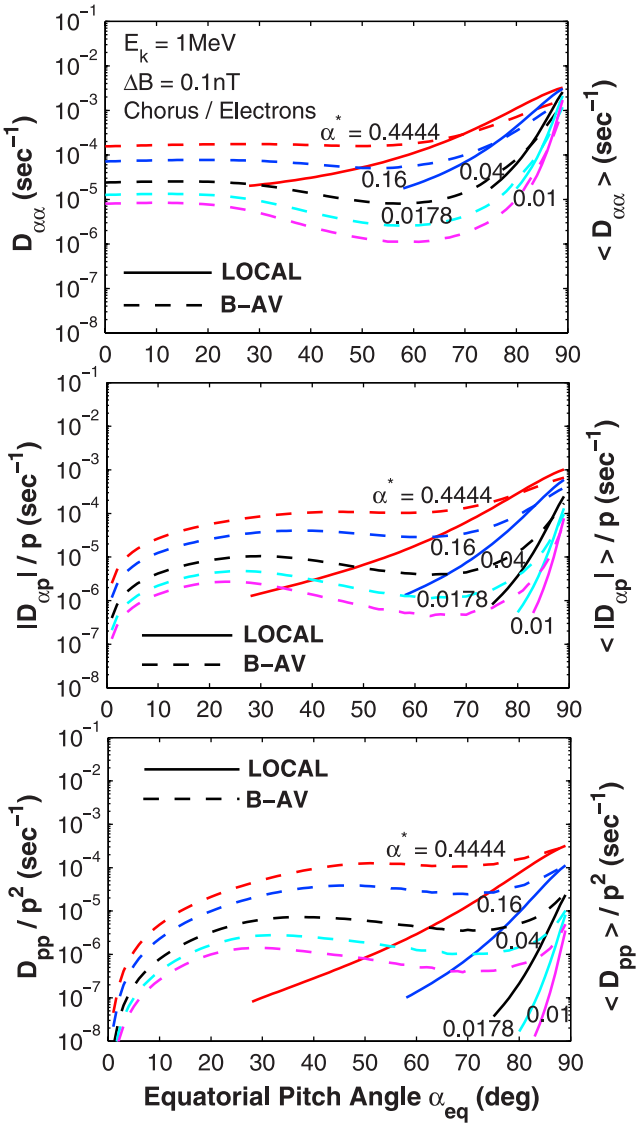

Figure 3. Local and bounce-averaged diffusion rates for electrons interacting with chorus, at $L = 4.5$, for the fixed energy of 1 MeV, and for the specified values of $\alpha^* = \Omega_e^2/\omega_{pe}^2$. Wave spectrum is as adopted in Figure 1.

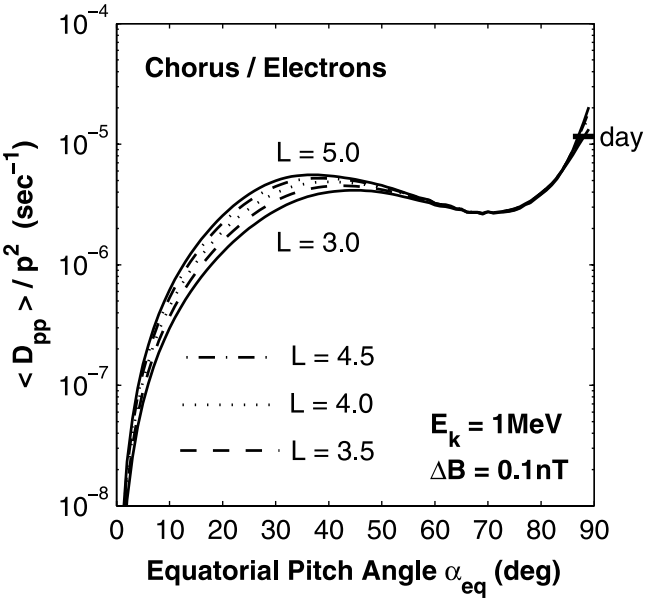

Figure 4. Bounce-averaged momentum diffusion rates for electrons interacting with chorus, for the fixed energy of 1 MeV, at the specified L values. Wave spectrum is as adopted in Figure 1, and 60% drift-averaging has been applied.

the equator, while for lower-energy electrons ($E_k \leq 100$ keV) the reverse is true. A good estimate for the electron loss timescale is given by $1/\langle D_{\alpha\alpha}\rangle$ where the bounce-averaged electron pitch angle diffusion coefficient $\langle D_{\alpha\alpha}\rangle$ is evaluated at the equatorial loss cone angle. The timescale for pitch angle scattering of 1 MeV electrons into the loss cone is less than 1 day, while the corresponding timescale for lower-energy electrons ($E_k \leq 100$ keV) is less than 1 hour. For electron energies up to 1 MeV, the local and bounce-averaged momentum diffusion rates tend to maximize at higher pitch angles. For 1 MeV electrons, bounce-averaging increases the diffusion rates and extends the range of pitch angles over which momentum diffusion is effective (Figures 1e and 1f and Figure 2, bottom). The momentum diffusion timescale for 1 MeV electrons with equatorial pitch angles in the range $30 < \alpha_{eq} < 90$ deg is less than 1 day.

[10] In Figure 3 we examine the sensitivity of the diffusion rates to variations in the electron density N_0, for 1 MeV electrons at $L = 4.5$. We assume that the waves are distributed latitudinally over the entire field line. We take the specified α^* values in the range $0.01 \leq \alpha^* \leq 0.4444$ corresponding to the approximate number density range $114 \geq N_0 \geq 2.6$ cm^{-3}. The parameters adopted in Figure 3 were used in Figure 2 of *Summers* [2005]. The value of the parameter $\alpha^* = \Omega_e^2/\omega_{pe}^2$ is proportional to B_0^2/N_0, where B_0 is the background magnetic field, and N_0 is the electron number density. As the value of α^* increases, or the electron number density N_0 decreases, the bounce-averaged diffusion rates broadly increase (Figure 3). From Figure 3 (bottom) we see that, as for the local rates [*Summers*, 2005], the bounce-averaged momentum rates at high pitch angles increase by about 3 orders of magnitude as α^* is increased from 0.01 to 0.4444. The result that energy diffusion is more effective in regions of lower electron density was obtained by *Summers et al.* [1998] from an analysis of resonant diffusion curves in momentum space. For MeV electrons at sufficiently large equatorial pitch angle, at $L = 4.5$, timescales for momentum diffusion are less than 1 day if $\alpha^* > 0.04$. This condition, which corresponds to $\omega_{pe}/|\Omega_e| < 5$, is typically encountered at $L = 4.5$ during active conditions over a broad range of local times [*Meredith et al.*, 2003a]. Figure 3 (top) also shows that bounce-averaged pitch angle diffusion rates near the loss cone can increase

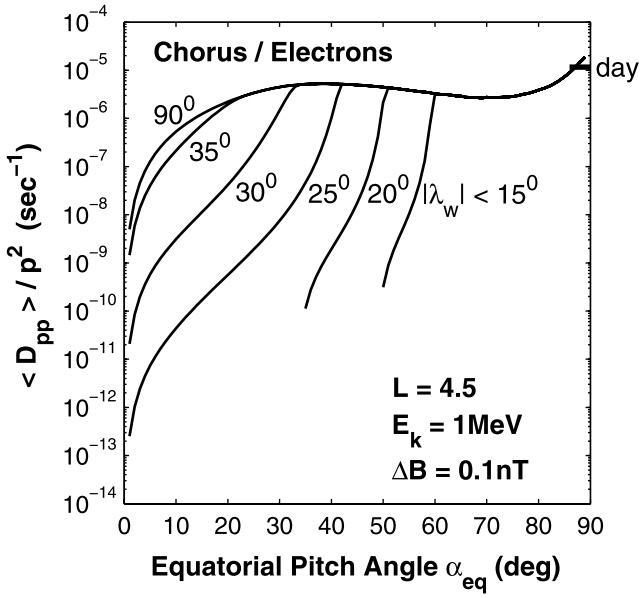

Figure 5. Corresponding to Figure 4, bounce-averaged momentum diffusion rates for electrons interacting with chorus, for the fixed energy of 1 MeV, at $L = 4.5$, for the indicated latitudinal distributions of waves.

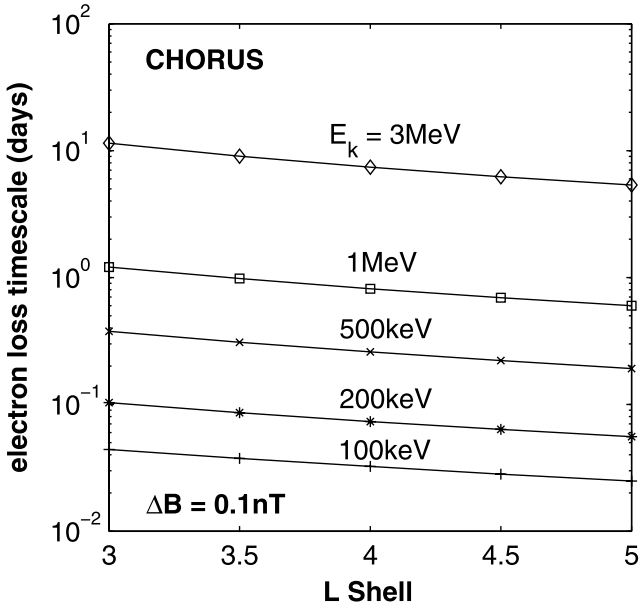

Figure 6. Electron loss timescales due to chorus scattering, as a function of L shell, for the specified energies. Wave spectrum is as adopted in Figure 4, and 60% drift-averaging has been applied.

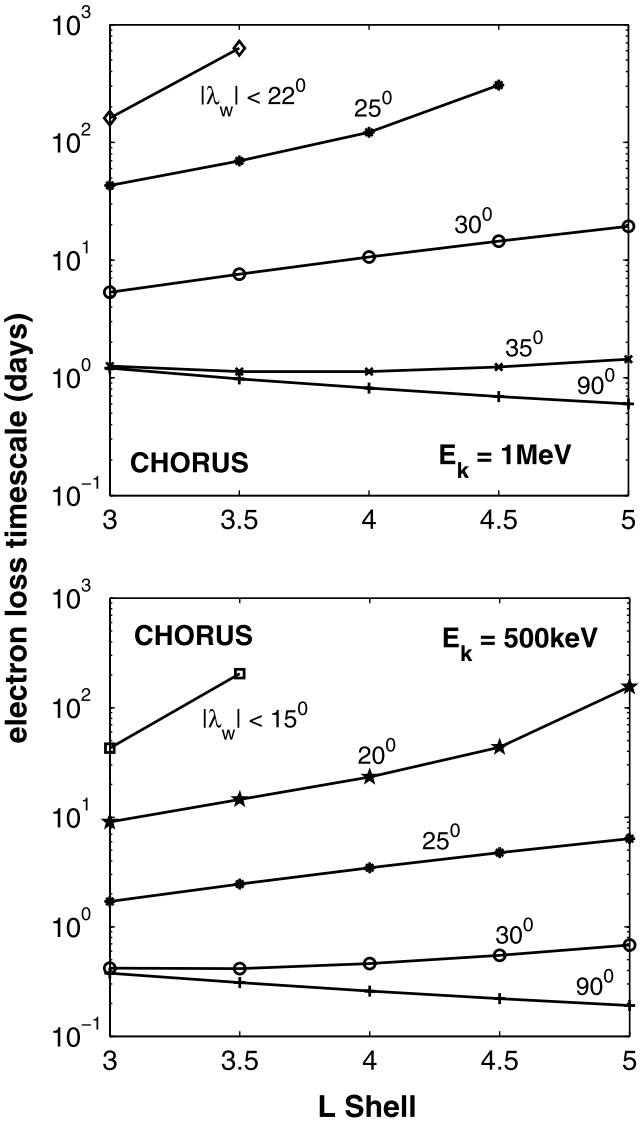

Figure 7. Corresponding to Figure 6, electron loss timescales, as a function of L shell, for the indicated latitudinal distributions of waves, and for the given energies.

significantly as the number density is decreased. Precipitation loss timescales for MeV electrons can be a few hours for the conditions assumed in Figure 3. MeV electron precipitation loss due to chorus scattering could therefore be important during the main phase of a storm when densities are low [*Thorne et al.*, 2005b].

[11] In Figure 4 we plot bounce-averaged momentum diffusion rates for MeV electrons at various L values. In this case, we assume that the waves are distributed latitudinally along the entire field line, and to simulate a typical MLT distribution of chorus waves we apply 60% drift-averaging. We also use the model due to *Sheeley et al.* [2001] for the density in the trough outside the plasmasphere, $N_0 = 124\ (3/L)^4\ \mathrm{cm}^{-3}$. We find that for such conditions, at sufficiently large equatorial pitch angles, the momentum diffusion timescale for MeV electrons is a few days or less and is largely independent of L shell. Bounce-averaged momentum diffusion rates for 1 MeV electrons at $L = 4.5$ are plotted in Figure 5 for various latitudinal distributions of chorus waves. We apply 60% drift-averaging, and we consider the distributions $|\lambda_W| < 15$, 20, 25, 30, 35, and 90 deg. For electrons with pitch angles in the range $60 < \alpha_{eq} < 90$ deg the momentum diffusion timescale is of the order of a few days if $|\lambda_W| < 15$ deg. Equatorial chorus waves can therefore effectively accelerate MeV electrons of sufficiently large pitch angle. If the latitudinal distribution of waves is increased from $|\lambda_W| < 15$ deg to $|\lambda_W| < 35$ deg, the range of pitch angles for effective acceleration (acceleration timescales of a few days) is increased to $20 < \alpha_{eq} < 90$ deg. Thus higher-latitude chorus ($|\lambda| > 15$ deg) increases the efficiency of the chorus mechanism for electron acceleration.

[12] In Figures 6 and 7 we plot electron loss timescales due to chorus scattering at the specified energies, as a function of L shell. As in Figure 5, we adopt the trough density model due to *Sheeley et al.* [2001], and we apply 60% drift-averaging. To estimate the loss timescale τ_{loss} due to chorus at $L = 3.0$, 3.5, 4.0, 4.5, and 5.0, we determine the quantity $\tau_{loss} = 1/\langle D_{\alpha\alpha}\rangle$, where $\langle D_{\alpha\alpha}\rangle$ is the bounce-averaged pitch angle diffusion coefficient for the specified chorus band evaluated at $\alpha_{eq} = (\alpha_L)_{eq}$, where $(\alpha_L)_{eq}$ is the equatorial loss cone angle given by equation (34) in the work of *Summers et al.* [2007]. In Figure 6 we assume that the chorus waves are distributed along the entire field line. For this case we see that the loss timescale τ_{loss} for 1 MeV electrons is about 1 day or less over the range $3 \leq L \leq 5$. Electrons of energy 500 keV are scattered even more efficiently ($\tau_{loss} \sim$ a few hours). In Figure 7 we show loss timescales for electrons of energies 1 MeV and 500 keV for the conditions assumed in Figure 6 except that we consider the effects of different latitudinal distributions of waves, as indicated. The results in Figure 7 show that for electrons of energy 500 keV to 1 MeV loss timescales due to chorus can be extremely sensitive to the latitudinal distribution of waves and also that efficient pitch angle scattering of such energetic electrons requires waves at higher latitudes. For instance, for MeV electrons (Figure 7, top) the loss timescale at $L = 5$ is about 20 days if $|\lambda_W| < 30$ deg but is slightly more than 1 day if $|\lambda_W| < 35$ deg. In agreement with the recent analysis of MeV electron microburst loss by *Thorne et al.* [2005b], our study finds that efficient scattering of MeV electrons by first-order cyclotron resonance with chorus typically requires waves with a latitudinal distribution $|\lambda_W| > 30$ deg.

[13] In this section, while we have considered various latitudinal distributions for chorus waves, we have assumed that the wave intensity is constant at latitudes over which waves are present. Chorus waves may undergo off-equatorial Landau damping [e.g., *Bortnik et al.*, 2006]. This would lead to a latitudinal dependence of the wave power. We do not take into account such an effect in the present investigation.

3. Interaction of Electrons With Plasmaspheric Hiss

[14] Plasmaspheric hiss is a broadband ELF whistler-mode emission in the frequency range from ~100 Hz to several kHz. Even during geomagnetically quiet periods, hiss is present and occupies a broad expanse of the plasma-

Table 1. Measured Values of the Electron Number Density N_0, the Parameter $\alpha^* = \Omega_e^2/\omega_{pe}^2$, and Average Hiss Amplitude ΔB From CRRES at the Specified L Values, in the Cases of Both Low and High Geomagnetic Activity[a]

				ΔB, pT		τ_{loss}, days		
L	N_0, cm^{-3}	α^*	E_{min}, keV	Equator	Midlatitude	214 keV	510 keV	1.09 MeV
Low Geomagnetic Activity								
3.0	1019	0.0126	41.1	34.5	34.5	0.19	0.73	3.14
3.5	584	0.0087	16.3	36.3	36.3	0.24	0.96	3.69
4.0	303	0.0076	8.1	29	29	0.43	1.64	6.13
4.5	176	0.0064	3.8	20.4	20.4	1.05	3.63	13.3
5.0	101	0.0059	1.9	19.5	19.5	1.19	4.02	14.6
High Geomagnetic Activity								
3.0	597	0.0216	67.97	57.2	49.9	0.15	0.29	1.5
3.5	298	0.0171	31.26	62.5	51.2	0.08	0.38	1.82
4.0	155	0.0148	15.52	40.7	73.3	0.1	0.26	0.96

[a] E_{min} is the electron minimum resonant energy and τ_{loss} is the model calculation of the electron loss timescale due to hiss.

sphere. Plasmaspheric hiss intensifies during storms or substorms [*Smith et al.*, 1974; *Thorne et al.*, 1974]. The spatial extent of the plasmasphere depends on geomagnetic activity, with the innermost boundary of the plasmasphere located at $L = 2$ or 3 during storms and at $L = 5$ or 6 during quiet periods. Hiss can also occur outside the plasmasphere, e.g., in detached plasma regions [e.g., *Parrot and Lefeuvre*, 1986]. Typical broadband amplitudes of hiss range from 10 pT during quiet periods [*Tsurutani et al.*, 1975] to 100 pT during the recovery phase of storms [*Smith et al.*, 1974]. *Meredith et al.* [2004] carried out a statistical analysis of plasmaspheric hiss ($100 < f < 2000$ Hz) using wave data and particle data from CRRES. Hiss amplitudes were found to depend on L shell, MLT, magnetic latitude, and substorm activity. Further, it was discovered that hiss occurs in particular equatorial and midlatitude zones, primarily on the dayside. *Meredith et al.* [2004] found that during active conditions, equatorial hiss ($|\lambda| < 15$ deg) has an average amplitude $\Delta B = 40$ pT in the region $2 < L < 4$ from 0600 to 2100 MLT, while midlatitude hiss ($15 < |\lambda| < 30$ deg) has an average amplitude $\Delta B = 47$ pT in the region $2 < L < 4$ from 0800 to 1800 MLT. Midlatitude hiss was also found to extend beyond $L = 6$ from 1200 to 1500 MLT.

[15] There have been extensive observations of plasmaspheric hiss since the 1960s, e.g., see the review by *Hayakawa and Sazhin* [1992] and the references given by *Meredith et al.* [2004] and *Masson et al.* [2004]. Nevertheless, the generation mechanism of hiss has not been completely resolved. *Kennel and Petschek* [1966] originally proposed that plasmaspheric hiss can be produced by the electron cyclotron resonance instability. Various studies [e.g., *Church and Thorne*, 1983; *Solomon et al.*, 1988; *Cornilleau-Wehrlin et al.*, 1993] have shown that hiss can be excited from anisotropic distributions of electrons that have been injected into the inner magnetosphere from the plasmasheet during substorms. Whether significant wave amplification can be achieved by the cyclotron resonance generation mechanism, however, is not clear, and further detailed modeling needs to be carried out. *Meredith et al.* [2004] found that enhanced equatorial and midlatitude emissions are associated with electron flux enhancements in the energy range of 10s to 100s of keV, which suggests that these electrons are the most likely source of plasmaspheric hiss. The study of *Meredith et al.* [2004] suggests that plasmaspheric hiss could be generated in two source regions, one near the equator and the other at midlatitude.

[16] *Lyons et al.* [1972] showed that pitch angle scattering of energetic electrons into the loss cone by plasmaspheric hiss can explain the formation of the quiet-time slot region that separates the inner ($1 < L < 2.5$) and outer ($3 < L < 7$) radiation belts. Plasmaspheric hiss also contributes to the pitch angle scattering loss to the atmosphere of relativistic (>1 MeV) electrons generated during the recovery phase of magnetic storms [*Tsurutani et al.*, 1975; *Albert*, 1994, 2003; *Thorne et al.*, 2005a]. However, since hiss occurs in the high density ($\sim 10^3$ cm^{-3}) plasmasphere, the parameter $\alpha^* \propto B_0^2/N_0$ is small, and, consequently, from the study of *Summers et al.* [1998], it follows that plasmaspheric hiss is not expected to be significant for electron acceleration.

[17] The fluxes of energetic electrons in the Earth's outer radiation belt gradually decay to quiet-time levels following enhanced geomagnetic activity. *Meredith et al.* [2006] used CRRES observations to estimate the timescales for energetic electron loss. It was found that the loss of electrons in the region $3 \leq L \leq 5$ occurs on timescales ranging from 1.5 to 3.5 days for 214 keV electrons and 5.5 to 6.5 days for 1.09 MeV electrons. Further, *Meredith et al.* [2006] found that electron decay takes place in regions where $\alpha^* = \Omega_e^2/\omega_{pe}^2$ is small (<0.02), which indicates that the loss of electrons takes place in the plasmasphere. Loss timescales for pitch angle scattering by plasmaspheric hiss were calculated using wave properties deduced from the CRRES observations and the theoretical framework of *Lyons et al.* [1972] and *Albert* [1994]. *Meredith et al.* [2006] concluded that plasmaspheric hiss propagating at small wave-normal angles is responsible for electron loss over a wide range of energies and L shells. Plasmaspheric hiss at large wave-normal angles was not found to contribute significantly to the electron loss rates.

[18] Here, we use the theoretical formalism in *Summers et al.* [2007] to estimate timescales for energetic electron loss from the outer radiation belt due to pitch angle scattering by plasmaspheric hiss in both regimes of low and high geomagnetic activity. We assume that hiss has a Gaussian frequency distribution, with lower-frequency $\omega_1/2\pi = 0.1$ kHz, upper-frequency $\omega_2/2\pi = 2.0$ kHz, bandwidth $\delta\omega/2\pi = 0.3$ kHz, and $\omega_m/2\pi = 0.55$ kHz as the frequency of maximum wave power. In the upper part of Table 1, for low geomagnetic activity ($K_p < 3^-$), we present values for the electron number density N_0, the parameter $\alpha^* = \Omega_e^2/\omega_{pe}^2$, and the mean hiss amplitude ΔB, from CRRES data given by *Meredith et al.* [2006] at $L = 3.0$, 3.5, 4.0, 4.5, and 5.0. We also give the corresponding electron minimum resonant energy E_{min} at these L values, as calculated from equation (16) in the work of *Summers et al.* [2007] with $\sigma = e$ and $s = 1$. In Figure 8 we show the local hiss diffusion coefficients $D_{\alpha\alpha}$ and corresponding bounce-averaged diffusion coefficients $\langle D_{\alpha\alpha} \rangle$, at $L = 3.0$, 3.5, 4.0, 4.5, and 5.0, for the electron energies $E_k = 214$ keV, 510 keV, and 1.09 MeV. The coefficients $D_{\alpha\alpha}$ and $\langle D_{\alpha\alpha} \rangle$ are evaluated from equations (5) and (30) in the work of *Summers et al.* [2007] using the data corresponding to low geomagnetic activity given in Table 1. Figure 8 demonstrates generally that the efficiency of pitch angle scattering by hiss increases as the electron energy decreases and also as the L shell

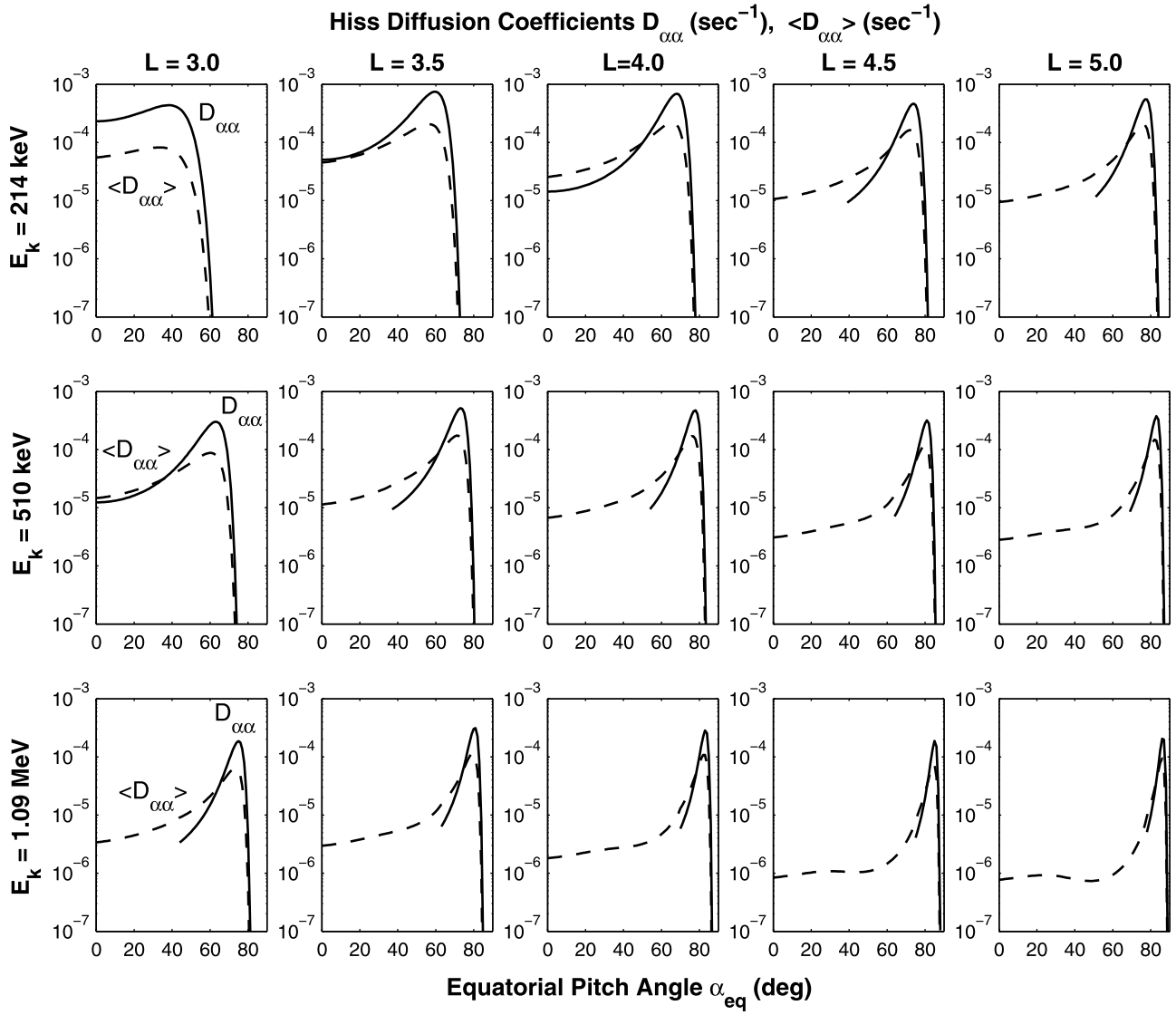

Figure 8. Local and bounce-averaged electron pitch angle diffusion coefficients due to hiss, at the given energies and L values, for parameters and wave amplitudes corresponding to low geomagnetic activity, as given in the upper part of Table 1.

decreases. Figure 8 also clearly shows the importance of performing bounce-averaging in order to obtain the effective scattering rates. For instance, for $3 \leq L \leq 5$, 1.09 MeV electrons at small equatorial pitch angles are not subject to resonant scattering. However, the bounce-averaged diffusion rates for 1.09 MeV electrons are significant near the equatorial loss cone, due to higher-latitude scattering. In general, the results of bounce-averaging depend on L value and particle energy. Bounce-averaging may increase, decrease, or leave unchanged the local scattering rate at the equator.

[19] In Figure 9, for each energy E_k = 214 keV, 510 keV, and 1.09 MeV, we plot local electron scattering rates as a function of magnetic latitude, at the specified L values, evaluated at the equatorial loss cone angle. Figure 9 illustrates that resonant pitch angle scattering occurs at progressively higher ranges of magnetic latitude as the L value is increased, for a fixed energy, or as the energy is increased, for a fixed L value. For example, for 1.09 MeV electrons near the equatorial loss cone, the range of effective scattering is approximately $15 < \lambda < 30$ deg at $L = 3$ and approximately $30 < \lambda < 40$ deg at $L = 5$. In Figure 10 (bottom) we plot the local scattering rates for 1.09 MeV electrons at $L = 3$ at the specified magnetic latitudes, as a function of equatorial pitch angle. For comparison, in Figure 10 (top) we show the corresponding bounce-averaged scattering rate. Figure 10 shows that near the equator at $L = 3$ the range of pitch angles over which 1.09 MeV electrons are in resonance with hiss is approximately $43 < \alpha_{eq} < 80$ deg, in agreement with Figure 8 (bottom). As the latitude is increased, the maximum scattering rate decreases and shifts to lower equatorial pitch angles. A similar scenario for MeV electron scattering by chorus waves was found by *Thorne et al.* [2005b].

[20] In Figure 11 we show electron loss timescales at the specified energies as a function of L corresponding to low geomagnetic activity. The measured values obtained from CRRES Medium Electrons A data by *Meredith et al.* [2006] are denoted by vertical lines. Theoretical values for the loss timescales found by *Meredith et al.* [2006] are plotted for

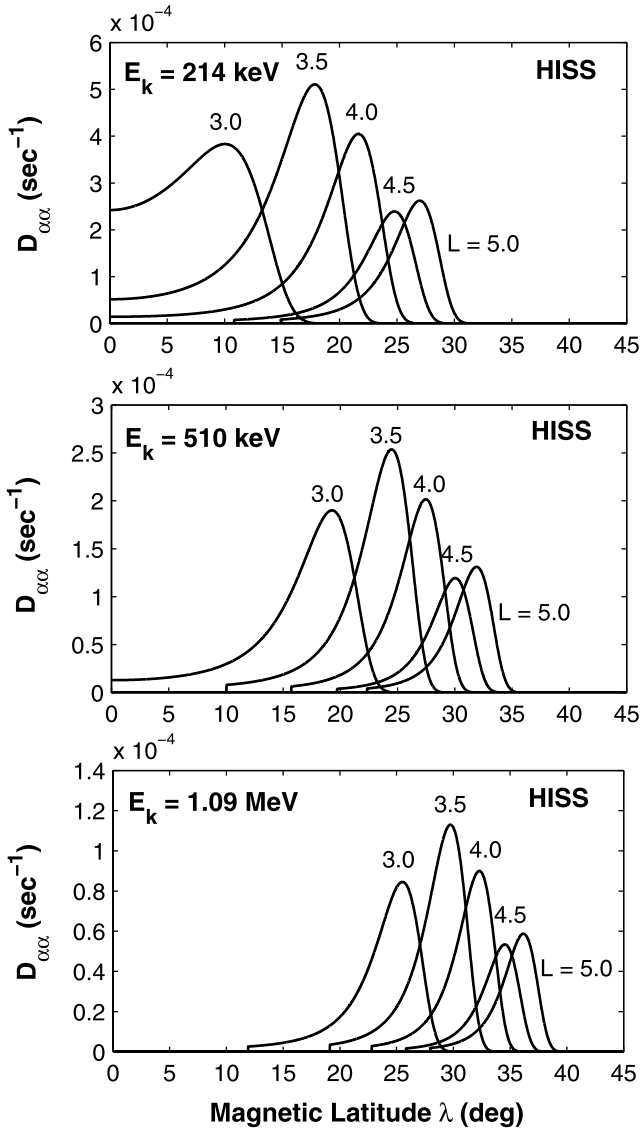

Figure 9. Local electron pitch angle diffusion coefficients due to hiss as a function of magnetic latitude λ, for the specified energies and L values, evaluated at the equatorial loss cone angle, for low geomagnetic activity, as in Figure 8.

wave-normal angles of Ψ_m = 0, 52, and 80 deg. Our own model values for the electron loss timescales τ_{loss} at L = 3.0, 3.5, 4.0, 4.5, and 5.0 are connected by solid lines. Our results for τ_{loss} are also given in Table 1 (top). The calculations of *Meredith et al.* [2006] are based on wave-normal distributions given in their Table 2, while our calculations assume field-aligned waves with zero wave-normal distribution. *Meredith et al.* [2006] employ a model due to *Lyons et al.* [1972] that requires the solution of a one-dimensional pitch angle diffusion equation for the electron distribution function. This equation and its associated boundary conditions are solved by *Meredith et al.* [2006] as a two-point boundary-value problem for the electron precipitation lifetime. Diffusion coefficient calculations by *Meredith et al.* [2006] were carried out using the PADIE code [*Glauert and Horne*, 2005]. In the present study we calculate the electron loss timescale using $\tau_{loss} = 1/\langle D_{\alpha\alpha}\rangle$, where the bounce-averaged diffusion coefficient $\langle D_{\alpha\alpha}\rangle$ is evaluated at the equatorial loss cone angle $(\alpha_L)_{eq}$ given by equation (34) in the work of *Summers et al.* [2007]. Our model solutions shown in Figure 11 generally provide a very good fit to the data. For electron energies E_k = 510 keV and 1.09 MeV our model solutions provide a slightly better fit to the data over the range $3 \leq L \leq 5$ than the solutions of *Meredith et al.* [2006]. For E_k = 214 keV and $3.5 \leq L \leq 5$, the small and medium wave-normal solutions of *Meredith et al.* [2006] provide a closer fit to the data than our model solutions. We conclude that at least for energies exceeding 500 keV, pitch angle scattering by field-aligned plasmaspheric hiss with a small spread in wave-normal angle can largely account for observed quiet-time electron losses over the range $3 \leq L \leq 5$. For E_k = 1.09 MeV and $4.5 \leq L \leq 5$,

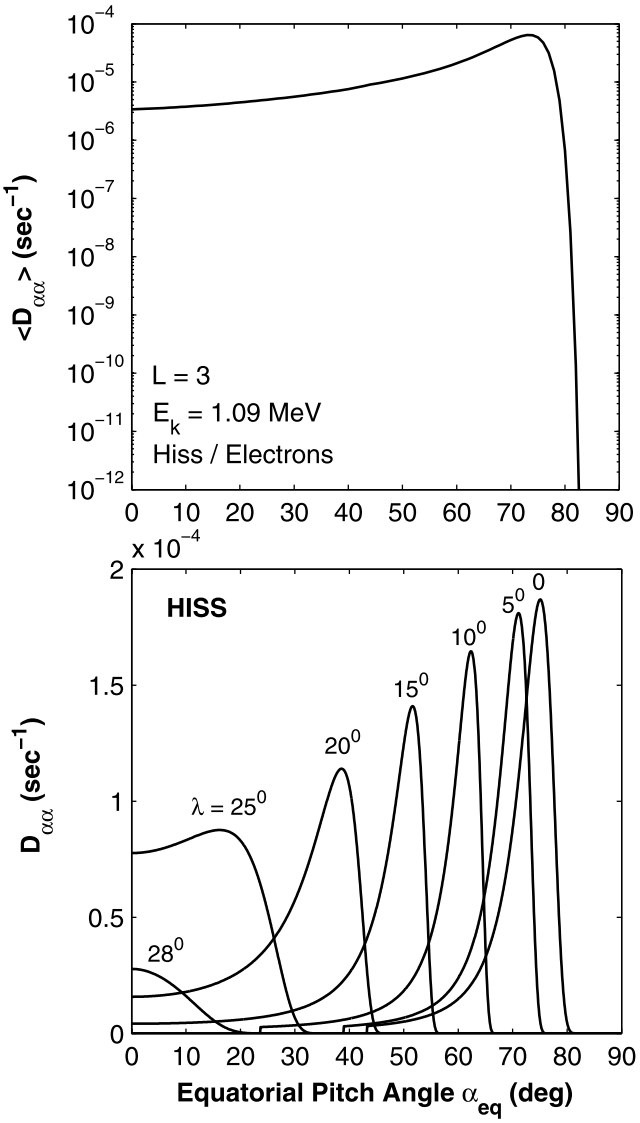

Figure 10. (bottom) Local electron pitch angle diffusion coefficients due to hiss as a function of equatorial pitch angle, for 1.09 MeV electrons at L = 3, at the given latitudes, for low geomagnetic activity and (top) corresponding bounce-averaged diffusion coefficient.

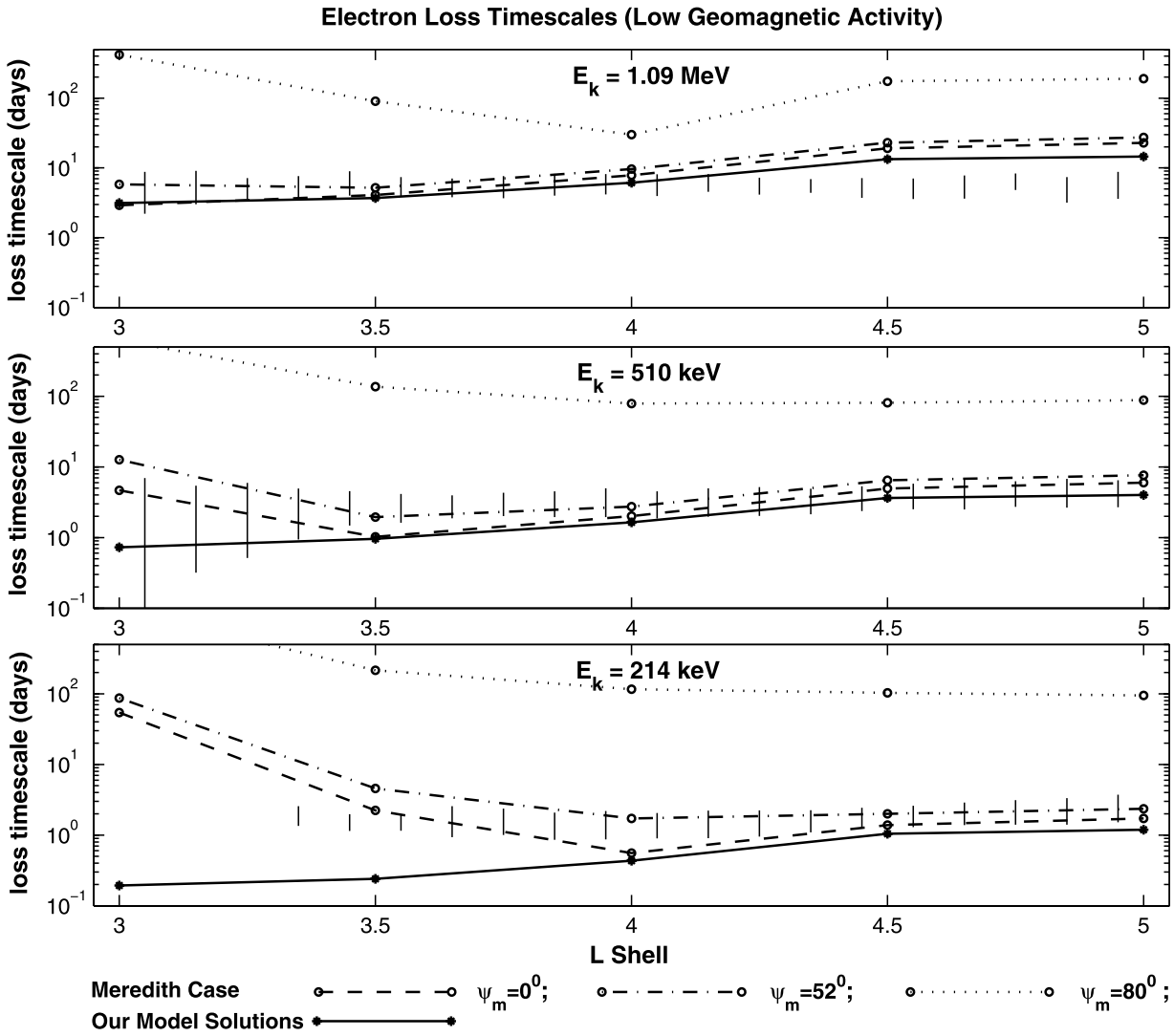

Figure 11. Electron loss timescales as a function of L at the specified energies for low geomagnetic activity. The measured values due to *Meredith et al.* [2006] are denoted by vertical lines. Our model calculations for the electron loss timescales due to hiss are shown together with the model values of *Meredith et al.* [2006]. All model solutions assume that the waves are distributed over the entire field line.

our model solutions and also those of *Meredith et al.* [2006] overestimate the loss timescales. As suggested by *Meredith et al.* [2006], it is possible that EMIC wave scattering could be important at MeV energies for larger L values ($L > \sim 4.5$).

[21] The model solutions of *Meredith et al.* [2006] and our model values shown in Figure 11 are based on the assumption that the waves are distributed latitudinally along the entire magnetic field line. We demonstrate the sensitivity of the loss timescales to the latitudinal wave distribution in Figure 12. For E_k = 1.09 MeV, we show loss timescales corresponding to waves distributed over the ranges $|\lambda_W| <$ 25, 30, 35, and 90 deg (top left), and we show the corresponding bounce-averaged diffusion coefficients at L = 4.5 (top right); similar results for E_k = 510 keV and 214 keV are shown in the middle and bottom. Figure 12 demonstrates that, dependent on electron energy and L shell, the loss timescales can be extremely sensitive to changes in the latitudinal wave distribution. For instance, examine the profiles for the loss timescales for the cases $|\lambda_W| < 25$ deg and $|\lambda_W| < 35$ deg, if E_k = 1.09 MeV; and the cases $|\lambda_W| <$ 15 deg and $|\lambda_W| < 30$ deg, if E_k = 510 keV. The nature of the dependence of the loss timescales on the latitudinal wave distribution is related to the range of latitude over which wave-particle resonance can take place, for a given energy and L value (as illustrated, for example, in Figures 9 and 10).

[22] In the lower part of Table 1, for high geomagnetic activity, we present values at L = 3.0, 3.5, and 4.0 for the electron number density N_0, the parameter $\alpha^* = \Omega_e^2/\omega_{pe}^2$, the electron minimum resonant energy $E_{\min}$, and the average amplitudes for equatorial ($|\lambda| < 15$ deg) and midlatitude ($15 < |\lambda| < 30$ deg) hiss. These values are derived from CRRES data over the MLT range from 0900 MLT through dusk to 2300 MLT, for geomagnetically active conditions specified by $AE^* > 500$ nT, where AE^* is defined as the maximum value of the AE index in the previous 3 hours. In Figure 13 we show our model calculations of electron loss timescales due to plasmaspheric hiss based on the parameter

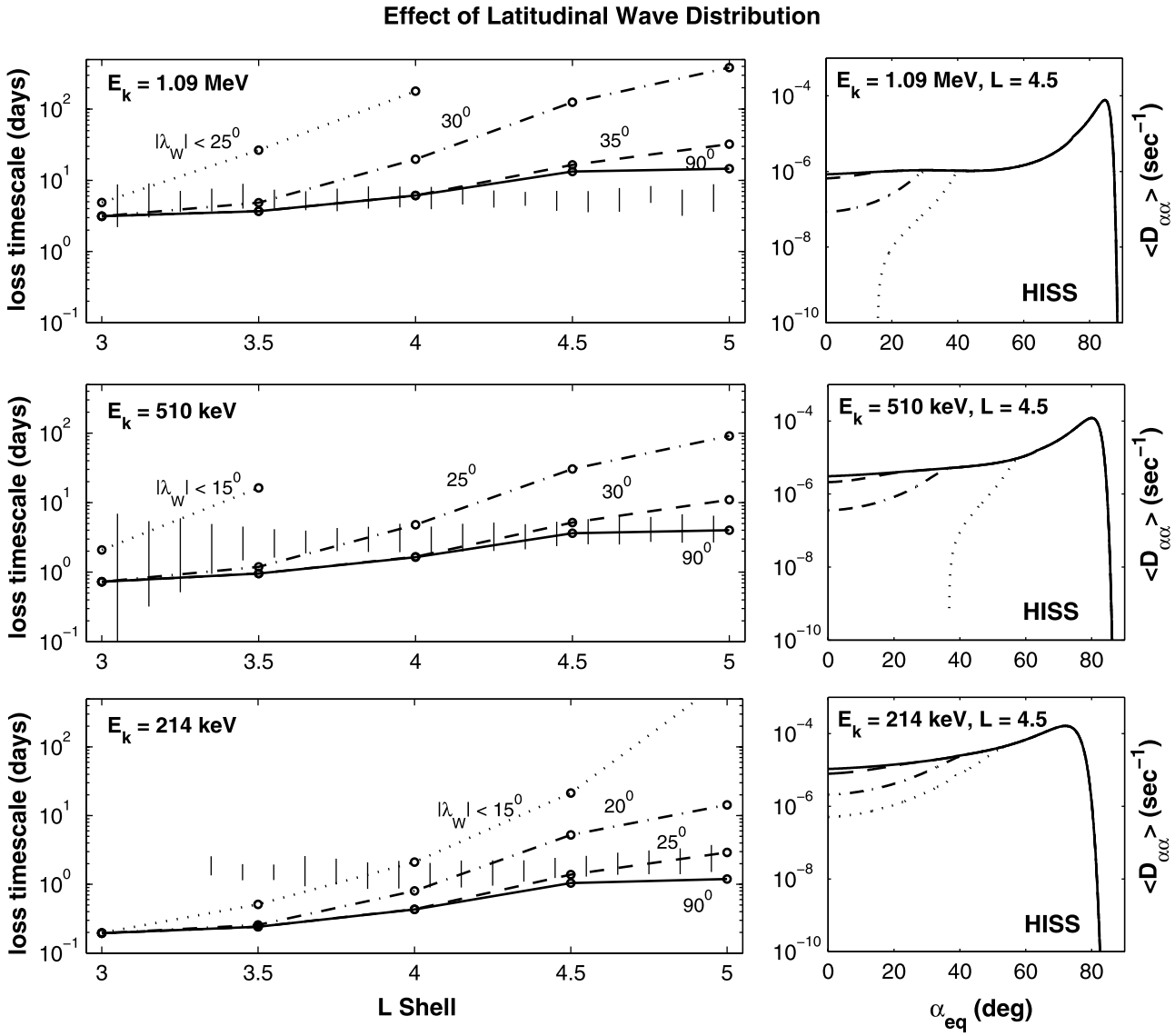

Figure 12. (left) Model calculations of the electron loss timescales for different latitudinal hiss distributions, at the specified energies and L values and (right) corresponding bounce-averaged pitch angle diffusion coefficients at $L = 4.5$ for the specified latitudinal hiss distributions. Measured loss timescales due to *Meredith et al.* [2006] are denoted by vertical lines on the left.

values and wave amplitudes for high geomagnetic activity given in Table 1. We assume the waves are distributed over the entire field line, and we take account of the specified MLT distribution by carrying out the required 14/24 drift-averaging. The electron loss timescales shown in Figure 13, given also in Table 1, confirm that pitch angle scattering by plasmaspheric hiss can provide an efficient mechanism for the precipitation loss of energetic electrons from the outer zone during geomagnetically active periods. We note that for $3 \leq L \leq 4$ and for all energies $E_k = 214$ keV, 510 keV, and 1.09 MeV, the electron loss timescale is less than 2 days. In particular, for electrons of energy 1.09 MeV at $L = 4$, the loss timescale is slightly less than 1 day. This implies that under certain conditions, hiss scattering can be comparable to EMIC wave scattering [*Summers and Thorne*, 2003; *Summers*, 2005] as a mechanism for depleting relativistic electrons from the outer radiation belt. During the main and early recovery phase of a typical magnetic storm, the plasmapause can move inward to $L = 3$, especially on the dawnside. However, the plasmapause tends to lie at a larger L shell on the duskside. This enables scattering by hiss to contribute to the loss of outer zone radiation belt electrons during the main and early recovery phase of a storm. In the following section, we will subsequently make a comparison (illustrated in Figure 18) of electron precipitation loss timescales due to scattering by plasmaspheric hiss and EMIC waves.

4. Interaction of Electrons With Electromagnetic Ion Cyclotron Waves

[23] Electromagnetic ion cyclotron (EMIC) waves in the frequency range 0.1–5.0 Hz are observed in the plasmasphere along the duskside plasmapause [*Fraser et al.*, 1996;

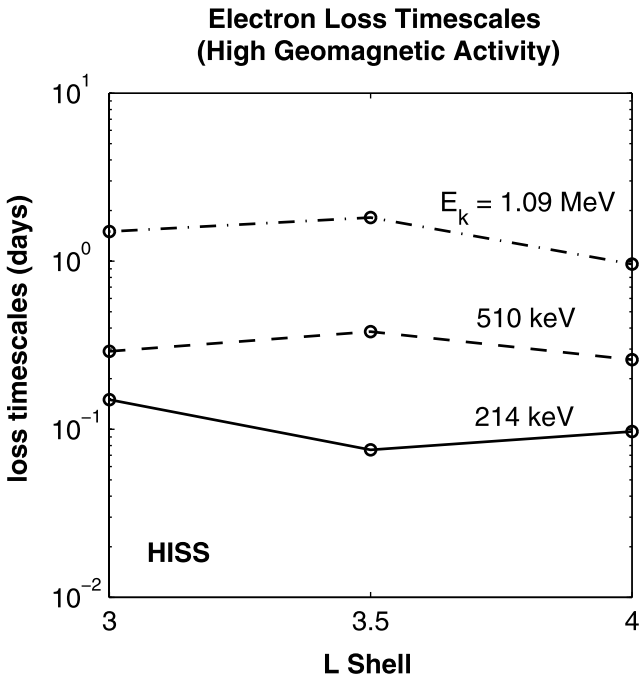

Figure 13. Model calculations of the electron loss timescales due to hiss at the specified energies and L values, for parameters and wave amplitudes corresponding to high geomagnetic activity, as given in the lower part of Table 1.

Jordanova et al., 2001] or within drainage plumes. The waves can be generated in three distinct bands below the hydrogen (H^+), helium (He^+), and oxygen (O^+) ion gyrofrequencies; examples of (L-mode) EMIC dispersion curves are given in section 3 of *Summers et al.* [2007]. EMIC waves are intensified during magnetic storms [*Fraser et al.*, 1996; *Bräysy et al.*, 1998; *Erlandson and Ukhorskiy*, 2001] with typical broadband amplitudes reaching values in the range 1–10 nT. A source of free energy for EMIC wave excitation is the anisotropic distribution of low-energy (~keV) ring current hydrogen (H^+) ions convected from the magnetotail [*Jordanova et al.*, 2001]. The particular band of EMIC waves that is excited depends on the ion composition, level of geomagnetic activity, and spatial location [*Fraser and Nguyen*, 2001].

[24] Even though the drift orbits of stormtime relativistic (>1 MeV) electrons intersect the localized zone of EMIC wave excitation briefly, significant electron pitch angle scattering and precipitation loss can occur over many drift orbits, namely several hours, because EMIC wave amplitudes typically exceed the level for strong diffusion scattering [*Summers et al.*, 1998; *Summers and Thorne*, 2003]. *Summers and Thorne* [2003] analyzed theoretically how the minimum energy for EMIC wave/electron resonant interaction depends on the parameter $\alpha^* = \Omega_e^2/\omega_{pe}^2$, the properties of the EMIC wave spectrum, and the ion composition. *Summers and Thorne* [2003] found that in order to lower electron resonant energies to geophysically interesting values, a suitably low value of the parameter α^* is required. Typically, $\alpha^* \leq 0.01$ is sufficient to ensure minimum electron resonant energies comparable to 1 MeV if other conditions also hold, e.g., if wave frequencies are just below the hydrogen or helium ion gyrofrequencies. The condition $\alpha^* \leq 0.01$ holds in regions of high electron density or low magnetic field such as the plasmasphere or within detached plasma regions at high L values. Since EMIC wave/electron resonance occurs in low-α^* regions, EMIC waves are not expected to be effective for electron acceleration [*Summers et al.*, 1998]. From a statistical study of more than 800 EMIC wave events observed on CRRES, *Meredith et al.* [2003c] reported a subset of L-mode events with minimum electron resonant energies below 2 MeV, confined to regions where $\alpha^* < 0.01$, for frequencies just below the hydrogen or helium ion gyrofrequencies. The EMIC wave average spectral intensity of 4–5 nT^2/Hz measured by *Meredith et al.* [2003c] is sufficient to cause electron pitch angle diffusion near the strong diffusion limit.

[25] We now examine electron pitch angle diffusion rates for EMIC waves in hydrogen and multi-ion plasmas. In Figure 14 we plot local and bounce-averaged electron diffusion coefficients for L-mode EMIC waves in a hydrogen plasma, at $L = 4$, for the specified energies. We set $\alpha^* = 2.3 \times 10^{-3}$ corresponding to the electron number density $N_0 = 1000$ cm^{-3}, characteristic of the plasmasphere. We assume a Gaussian frequency spectrum, with peak frequency $\omega_m = \Omega_p/3$, where Ω_p is the proton gyrofrequency, and we choose the waveband $\Omega_p/6 < \omega < \Omega_p/2$, with $\delta\omega = \Omega_p/6$. The parameter values used in Figure 14 are identical to those used to calculate the local pitch angle diffusion coefficients in Figure 4 of *Summers* [2005]. In Figure 14, to take account of the typical MLT distribution of EMIC waves in the plasmasphere, we have applied 1% drift-averaging. We have further assumed that the waves are distributed latitudinally over the entire field line. The effect of bounce-averaging is to reduce the pitch angle diffusion rates by about an order of magnitude for energies $E_k = 1.25$, 1.5, 2 MeV, and by about a factor of 3 for $E_k = 5$ MeV. Even

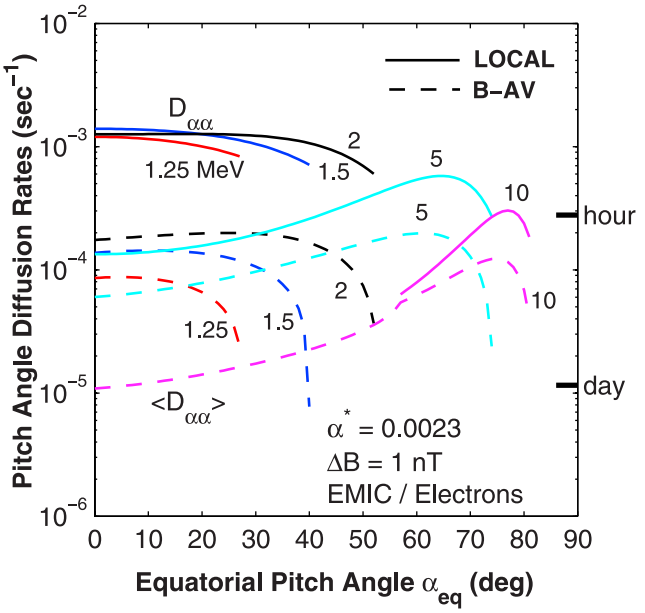

Figure 14. Local and bounce-averaged diffusion rates for L-mode EMIC waves interacting with electrons in a hydrogen plasma, at $L = 4$, for the indicated energies; 1% drift-averaging has been applied.

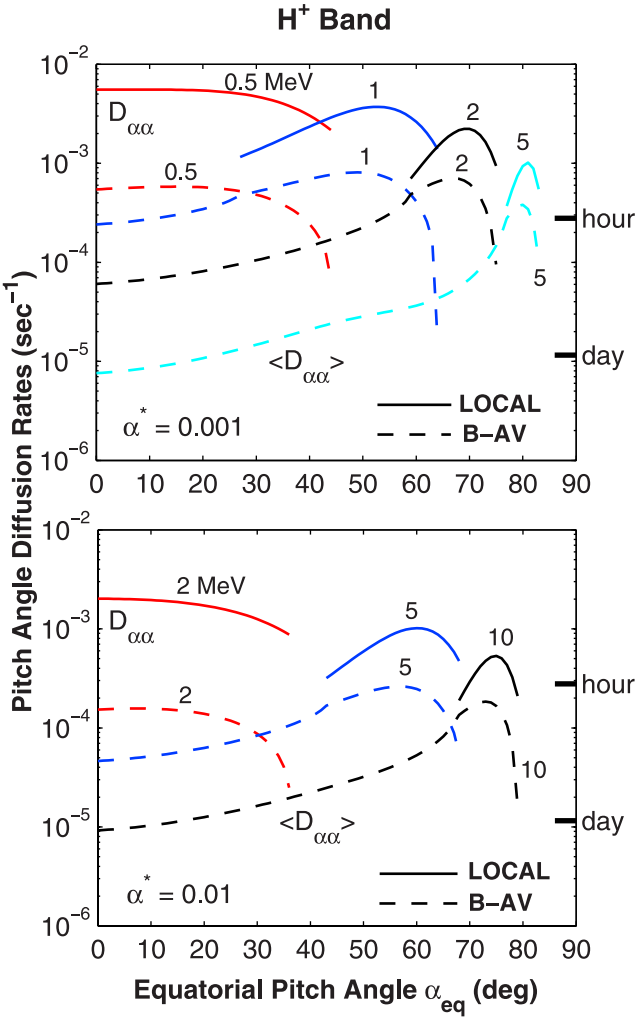

Figure 15. Local and bounce-averaged electron diffusion rates for hydrogen (H^+) band EMIC waves in a multi-ion plasma, at $L = 4$, for the indicated energies; wave amplitude $\Delta B = 1$ nT and 1% drift-averaging has been applied.

after both bounce-averaging and drift-averaging have been carried out, the pitch angle scattering rates of electrons of energies $E_k = 1.25$, 1.5, 2, 5 MeV near the equatorial loss cone correspond to rapid precipitation loss over a timescale of several hours. Near the equator, resonance with 10 MeV electrons is confined to the approximate pitch angle range $57 < \alpha_{eq} < 80$ deg. The effects of significant scattering at higher latitudes produce a scattering timescale for 10 MeV electrons near the loss cone ($\alpha_{eq} \sim 5$ deg) of about 1 day.

[26] In Figures 15, 16, and 17 we show local and bounce-averaged electron diffusion coefficients for L-mode EMIC waves in the hydrogen (H^+), helium (He^+), and oxygen (O^+) bands; drift-averaging of 1% has also been applied. In each figure we plot the pitch angle diffusion rates at $L = 4$, for the specified electron energies. To represent a range of electron number densities in the plasmasphere, we set $\alpha^* = 10^{-3}$ at the top and $\alpha^* = 10^{-2}$ at the bottom. The wave parameters and ion densities (η_1, η_2, η_3) adopted in Figures 15, 16, and 17 are those adopted by *Summers and Thorne* [2003] in their Figures 8, 9, and 10, respectively. In each case we set the wave amplitude $\Delta B = 1$ nT. The parameters adopted for the H^+ band waves (Figure 15), $\omega_1 = 0.5\Omega_p$, $\omega_2 = 0.7\Omega_p$, $\omega_m = 0.6\Omega_p$, $\delta\omega = 0.1\Omega_p$, $\eta_1 = 0.85$, $\eta_2 = 0.1$, and $\eta_3 = 0.05$, typify the sudden commencement phase of a magnetic storm [*Bräysy et al.*, 1998]. Electron minimum resonant energies in the top and bottom of Figure 15 are 292 keV and 1.52 MeV, respectively. From Figure 15 (top) we see that the bounce-averaged scattering timescale near the equatorial loss cone for 1 MeV electrons is about 1 hour, and the timescale for 500 keV electrons is about 0.5 hour. We deduce from the top and bottom of Figure 15 that H^+ band waves can induce the rapid removal of relativistic (1–2 MeV) electrons from the outer zone in a timescale of a few hours.

[27] In Figure 16, for the helium (He^+) band, we use parameters representative of the main phase and recovery phase of a storm ($\omega_1 = 2.5\Omega_{O+}$, $\omega_2 = 3.5\Omega_{O+}$, $\omega_m = 3\Omega_{O+}$, $\delta\omega = 0.5\Omega_{O+}$, where Ω_{O+} is the oxygen ion gyrofrequency; $\eta_1 = 0.7$, $\eta_2 = 0.2$, and $\eta_3 = 0.1$). Electron minimum resonant energies in the top and bottom of Figure 16 are 819 keV and

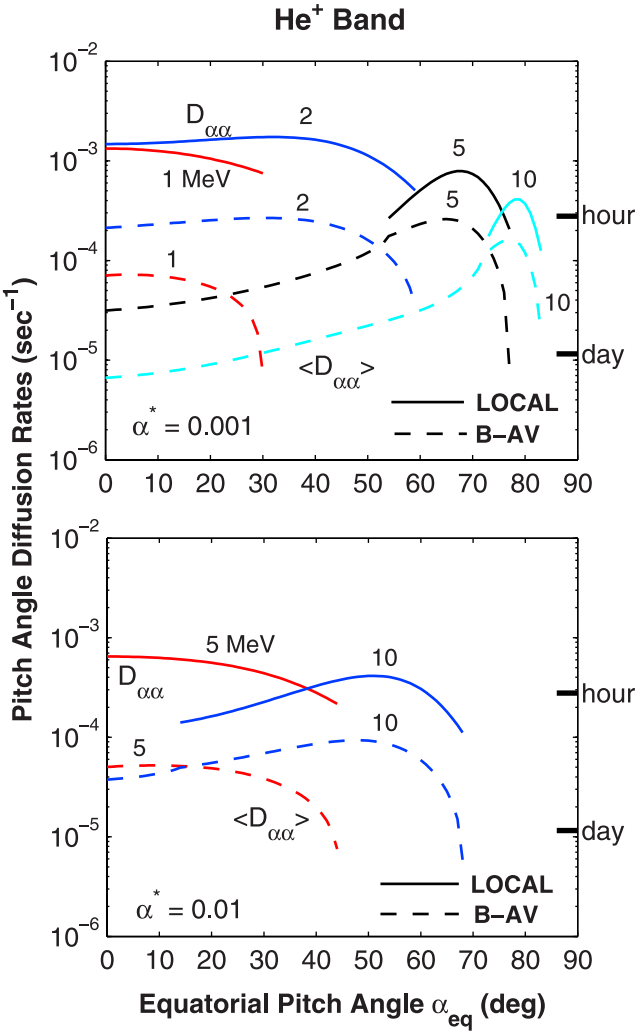

Figure 16. Local and bounce-averaged electron diffusion rates for helium (He^+) band EMIC waves in a multi-ion plasma, at $L = 4$, for the indicated energies; wave amplitude $\Delta B = 1$ nT and 1% drift-averaging has been applied.

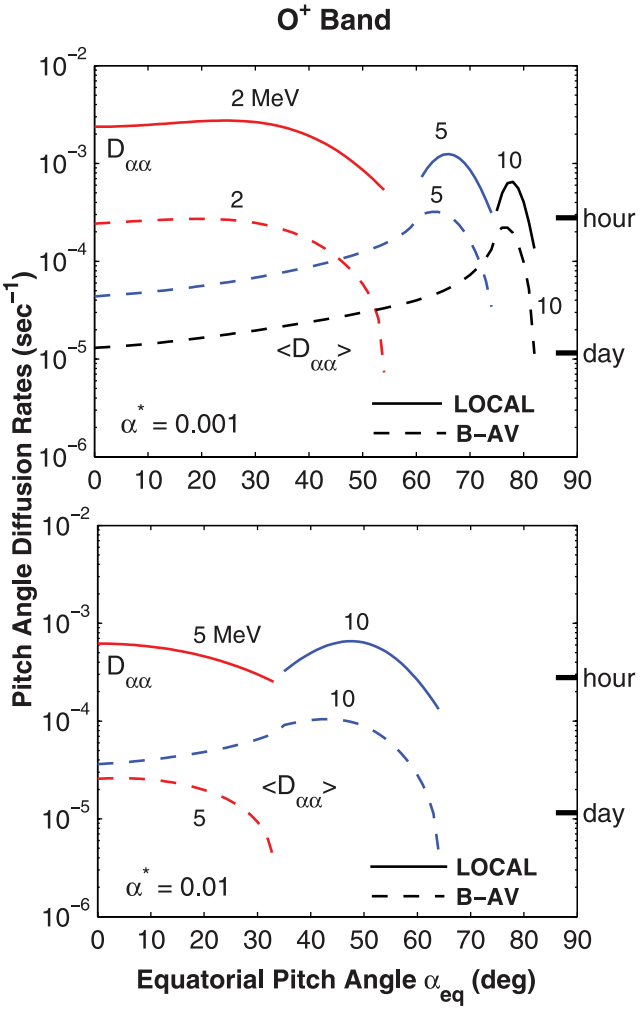

Figure 17. Local and bounce-averaged electron diffusion rates for oxygen (O^+) band EMIC waves in a multi-ion plasma, at $L = 4$, for the indicated energies; wave amplitude $\Delta B = 1$ nT and 1% drift-averaging has been applied.

3.4 MeV, respectively. The timescale for removing relativistic electrons (of energies one to several MeV) from the outer zone by He^+ band scattering during storms can be several hours (Figure 16), comparable to the loss timescale due to H^+ band scattering (Figure 15). X-ray observations of MeV electron precipitation from balloons reported by *Lorentzen et al.* [2000] and *Millan et al.* [2002] can be explained by such EMIC wave scattering. Scattering rates for oxygen (O^+) band waves are shown in Figure 17 for parameters representative of the main phase of a storm ($\omega_1 = 0.85\Omega_{O+}$, $\omega_2 = 0.95\Omega_{O+}$, $\omega_m = 0.9\Omega_{O+}$, $\delta\omega = 0.05\Omega_{O+}$, $\eta_1 = 0.6$, $\eta_2 = 0.2$, $\eta_3 = 0.2$). O^+ band waves typically cannot scatter MeV electrons since the minimum electron resonant energy exceeds 1 MeV. When present, O^+ band waves can be expected to cause rapid scattering loss of electrons at higher relativistic energies, 5–10 MeV (Figure 17, bottom).

[28] In Figure 18 (left) we show electron loss timescales due to EMIC wave scattering at $L = 3.0$, 3.5, 4.0, 4.5, 5.0, at the specified energies in the range 0.9–5 MeV; for comparison we also show corresponding electron loss timescales due to scattering by plasmaspheric hiss. We assume a hydrogen plasma and we use the plasmaspheric density model of *Sheeley et al.* [2001], $N_0 = 1390\ (3/L)^{4.83}$ cm^{-3}. For the EMIC waves we take $\omega_1 = 0.2\Omega_p$, $\omega_2 = 0.7\Omega_p$, $\omega_m = 0.45\Omega_p$, $\delta\omega = 0.25\Omega_p$, $\Delta B = 1$ nT, and we perform 1% drift-averaging. For the hiss, we take $\omega_1/2\pi = 0.1$ kHz, $\omega_2/2\pi = 2.0$ kHz, $\omega_m/2\pi = 0.55$ kHz, and $\delta\omega/2\pi = 0.3$ kHz, $\Delta B = 0.1$ nT, and we perform 60% drift-averaging. The electron loss timescale τ_{loss} is calculated using $\tau_{loss} = 1/\langle D_{\alpha\alpha}\rangle$, evaluated at the equatorial loss cone angle $(\alpha_L)_{eq}$. For the conditions adopted in Figure 18, we see that over the energy range 0.9–5 MeV, electron loss timescales range, where scattering occurs, from about 1 hour to several hours, dependent on L value; EMIC waves scatter 1 MeV electrons only in the range $4 \le L \le 5$, but scatter electrons of energy 1.5–5 MeV throughout the range $3 \le L \le 5$. The hiss amplitude $\Delta B = 100$ pT assumed in Figure 18 is characteristic of intense geomagnetic activity. In this case, loss timescales due to hiss for 1 MeV electrons are less than 1 day over the range $3 \le L \le 5$; and for electrons of energy 1.2–2 MeV the loss timescales due to hiss are in the approximate range 1–4 days. Hiss can therefore be expected to contribute significantly to relativistic (1–2 MeV) electron loss during the recovery phase of a magnetic storm. We note that scattering loss timescales due to hiss and EMIC waves can be comparable, for example for 900 keV electrons at $L = 4.5$. Since minimum resonant energies for hiss/electron interactions are generally low, in certain regimes hiss can be more effective for inducing scattering loss than EMIC waves. For instance, in Figure 18, for $E_k = 1$–1.2 MeV and $3 \le L \le 4$, timescales for loss due to hiss are less than or of the order of 1 day, while EMIC waves do not scatter electrons in this regime.

[29] In Figure 18 (right), for EMIC waves, we plot local scattering rates as a function of magnetic latitude, at the specified energies and L values, for electrons at the equatorial loss cone. From Figure 18 we observe that 1 MeV electrons near the equatorial loss cone are in resonance with EMIC waves only over the narrow latitude range $|\lambda| < 5$ deg, while the corresponding scattering range for 5 MeV electrons is about $|\lambda| < 20$ deg. For relativistic electrons near the equatorial loss cone ($\alpha_{eq} \sim 5$ deg), significant scattering by EMIC waves does not occur at high latitudes ($|\lambda| > 20$ deg).

[30] For comparison with the electron loss timescales due to EMIC wave scattering in a hydrogen plasma (Figure 18), we plot in Figure 19 electron loss timescales for hydrogen (H^+), helium (He^+), and oxygen (O^+) band waves. For Figure 19, the wave parameters adopted are exactly those used in Figures 15–17, and we apply 1% drift-averaging and assume the plasmaspheric density variation $N_0 = 1390\ (3/L)^{4.83}$ cm^{-3} due to *Sheeley et al.* [2001]. Electron loss timescales for H^+ band waves in Figure 19 are rapid (<1 day), similar to those for EMIC waves in a hydrogen plasma (Figure 18). For the conditions assumed in Figure 19, He^+ band and O^+ band waves do not scatter electrons of energy 1.25–2 MeV, but effectively scatter the more energetic (4–5 MeV) relativistic electron population.

[31] It should be emphasized that electron minimum resonant energies and scattering rates can be very sensitive to the assumed EMIC wave spectral properties, the ion composition, and the value of the α*-parameter. Nevertheless, there is ample evidence in Figures 14–19 that EMIC waves can induce precipitation loss of relativistic electrons

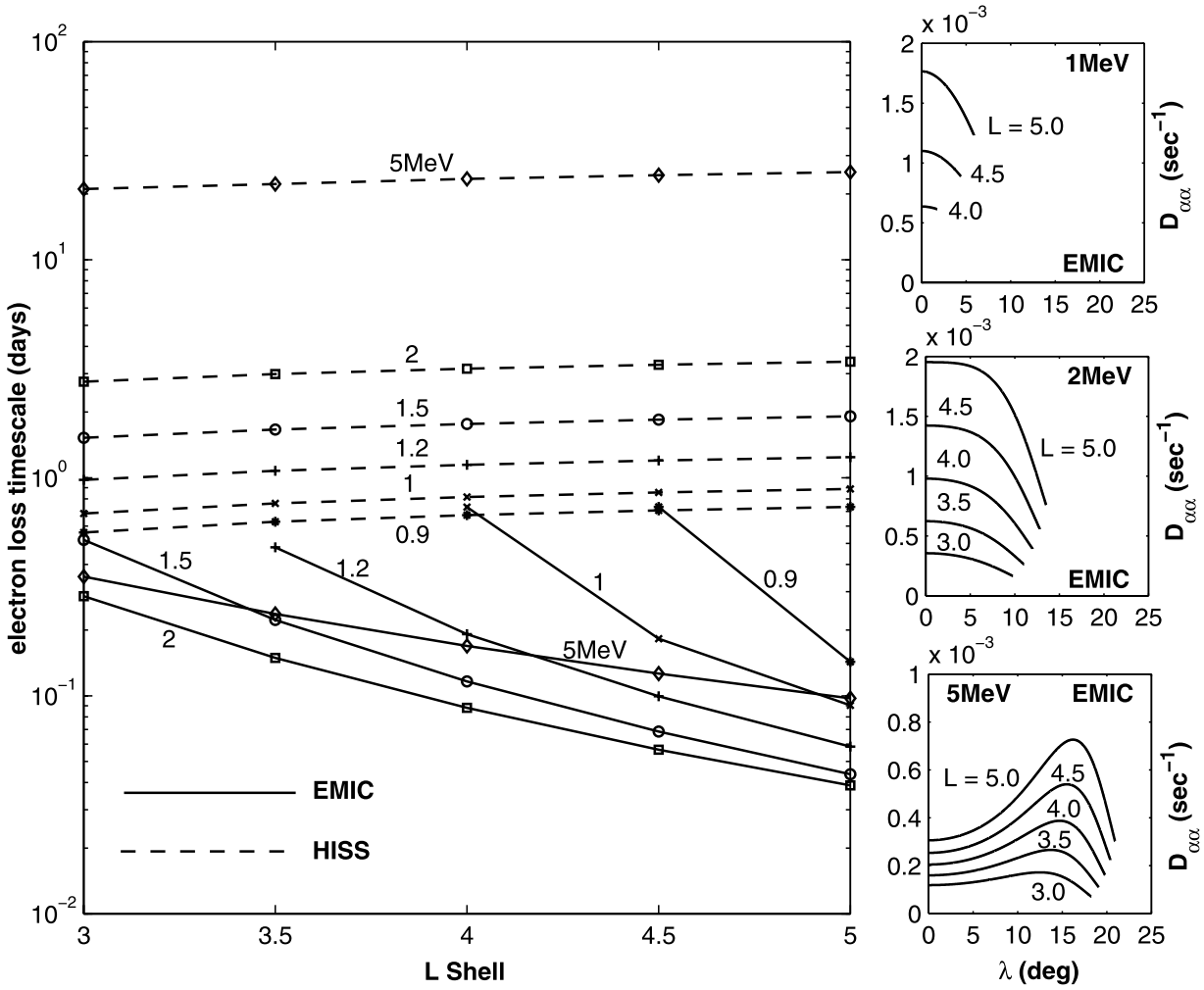

Figure 18. (left) Electron loss timescales due to EMIC waves and hiss in a hydrogen plasma, for the indicated energies. (right) Local diffusion rates as a function of magnetic latitude, for EMIC waves, at the indicated energies and L values, for electrons at the equatorial loss cone.

from the outer zone in a matter of hours under appropriate conditions. For electron resonance with EMIC waves, a general caveat is that even under optimal plasmaspheric conditions (in terms of background density and ion composition) resonant energies do not often go below 1 MeV; EMIC waves may therefore only be able to account for part of observed energetic electron losses. Rapid depletions of relativistic electron flux in the outer radiation belt reported by *Onsager et al.* [2002], *Green et al.* [2004], and recently by *Clilverd et al.* [2006] could at least be partly due to intense scattering by EMIC waves. EMIC waves could also contribute significantly to the well-known drop-out of energetic electrons that occurs during the main phase of a magnetic storm. The main-phase drop-out of relativistic electrons was originally attributed to the adiabatic "*Dst* effect" [*Li et al.*, 1997; *Kim and Chan*, 1997]. The estimates by *Loto'aniu et al.* [2006] of pitch angle scattering rates using measured EMIC wave spectra from CRRES further confirm that EMIC wave scattering can compete with the *Dst* effect as a mechanism for removing relativistic electrons from the outer zone during a storm main phase. It is evident from our calculations in sections 2, 3, and 4 that scattering by EMIC waves, whistler-mode chorus, or plasmaspheric hiss could separately, or in combination, cause large relativistic electron flux decreases in the outer radiation belt during geomagnetically active periods.

[32] In the present paper, and elsewhere in the literature, it has been stated that EMIC waves and plasmaspheric hiss are ineffective for electron acceleration. We demonstrate this in Figure 20, in which we plot bounce-averaged momentum diffusion rates for 1 MeV electrons, at $L = 4.5$, for typical chorus, hiss and EMIC wave parameters. For the chorus waves, we take $\omega_1 = 0.05\,|\Omega_e|$, $\omega_2 = 0.65\,|\Omega_e|$, $\omega_m = 0.35\,|\Omega_e|$, $\delta\omega = 0.15\,|\Omega_e|$, $\Delta B = 0.1$ nT, $\alpha^* = 0.16$, and we apply 60% drift-averaging. For hiss, we take $\omega_1/2\pi = 0.1$ kHz, $\omega_2/2\pi = 2.0$ kHz, $\omega_m/2\pi = 0.55$ kHz, $\delta\omega/2\pi = 0.3$ kHz, $\Delta B = 0.1$ nT, $\alpha^* = 0.001$ (or 0.01), and apply 60% drift-averaging. For the EMIC waves, we take $\omega_1 = 0.2\Omega_p$, $\omega_2 = 0.7\Omega_p$, $\omega_m = 0.45\Omega_p$, $\delta\omega = 0.25\Omega_p$, $\Delta B = 1$ nT, $\alpha^* = 0.001$, and we apply 1% drift-averaging. Optimal timescales for momentum diffusion of 1 MeV electrons at $L = 4.5$ are typically 1 day, 10 days, and

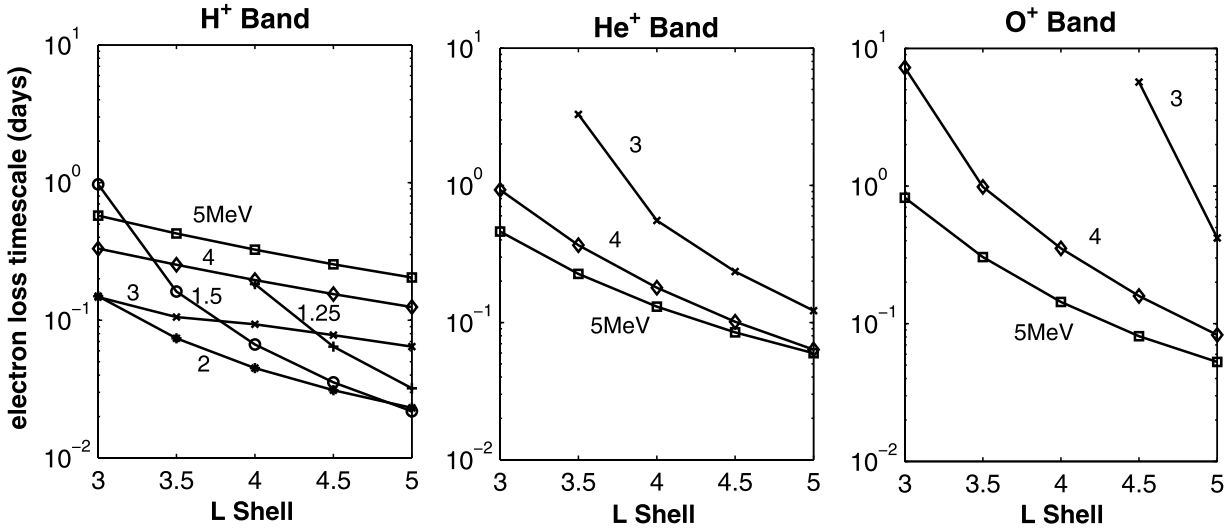

Figure 19. Electron loss timescales due to hydrogen (H^+) band, helium (He^+) band, and oxygen (O^+) band EMIC waves, for the indicated energies.

more than 10 days for chorus, hiss, and EMIC waves, respectively, as indicated in Figure 20.

5. Electron Loss Timescales Due to Combined Scattering By VLF Chorus, ELF Hiss, and EMIC Waves

[33] We consider the total (net) timescale for electron precipitation loss due to combined scattering by VLF chorus, ELF hiss, and EMIC waves, in the cases illustrated in Figure 21. The top left of Figure 21 is a schematic representation of the plasmasphere and typical distribution of waves for the case of high geomagnetic activity (case A). The top right schematically depicts the plasmasphere incorporating a drainage plume, together with an expected distribution of waves (case B). The boundary of the plasmasphere and plume shown in case B was constructed using Figure 5h of *Spasojevic et al.* [2003]. Parenthetically, we note the recent resurgence in studies of plasmaspheric plumes [e.g., *Spasojevic et al.*, 2003; *Moldwin et al.*, 2004; *Goldstein et al.*, 2004, 2005]. Specifically, we note that wave-particle interaction has been cited as an important loss process in plumes, in particular precipitation loss of energetic protons by EMIC wave scattering [*Burch et al.*, 2002; *Spasojevic et al.*, 2004; *Burch*, 2006]. Corresponding to each of cases A and B, we calculated the approximate percentage of an electron drift orbit that traverses each wave mode for a given L value. These results are shown in the tables in Figure 21. We define the total electron loss timescale τ_{tot} by the relation

$$\frac{1}{\tau_{tot}} = \frac{1}{\tau_{chorus}} + \frac{1}{\tau_{hiss}} + \frac{1}{\tau_{EMIC}} \tag{1}$$

where the timescales due to scattering by VLF chorus, ELF hiss, and EMIC waves (τ_{chorus}, τ_{hiss}, τ_{EMIC}) are calculated using

$$[\langle D_{\alpha\alpha}\rangle]_{chorus} = \frac{1}{\tau_{chorus}}, [\langle D_{\alpha\alpha}\rangle]_{hiss} = \frac{1}{\tau_{hiss}}, [\langle D_{\alpha\alpha}\rangle]_{EMIC} = \frac{1}{\tau_{EMIC}} \tag{2}$$

and each bounce-averaged diffusion coefficient is evaluated at the equatorial loss cone angle $(\alpha_L)_{eq}$. In calculating the diffusion coefficients in (2), we apply the drift-average percentage for each wave mode given in the tables in Figure 21. We assume each wave mode has a Gaussian spectral density and is distributed along the entire field line. For chorus, we assume the waveband $0.05\,|\Omega_e| < \omega < 0.65\,|\Omega_e|$, with $\omega_m = 0.35\,|\Omega_e|$, $\delta\omega = 0.15\,|\Omega_e|$, and amplitude ΔB = 0.1 nT. For hiss, we assume a waveband with lower-frequency $\omega_1/2\pi$ = 0.1 kHz, upper-frequency $\omega_2/2\pi$ = 2.0 kHz, with bandwidth $\delta\omega/2\pi = 0.3$ kHz, $\omega_m/2\pi = 0.55$ kHz, and amplitude ΔB = 0.1 nT. For EMIC waves, we assume the waveband $\Omega_p/6 < \omega < \Omega_p/2$, with $\omega_m = \Omega_p/3$, $\delta\omega = \Omega_p/6$, and amplitude ΔB = 1 nT. Following *Sheeley et al.* [2001], we assume the density variation $N_0 = 1390\ (3/L)^{4.83}$ cm^{-3}

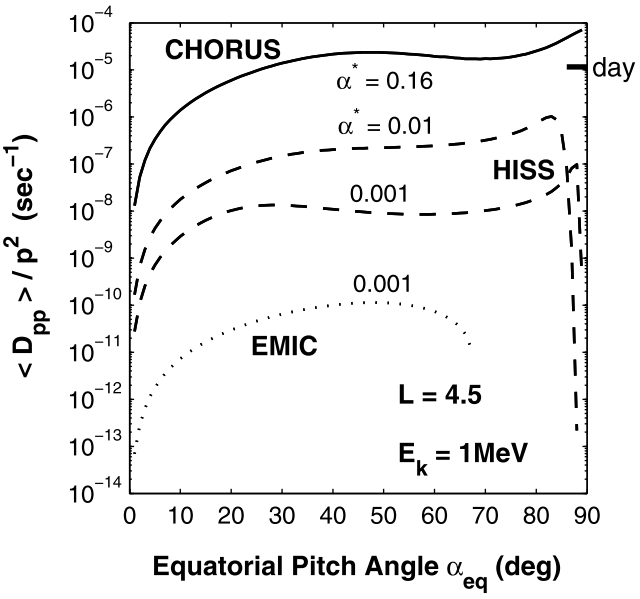

Figure 20. Comparison of bounce-averaged momentum diffusion rates for 1 MeV electrons at L = 4.5 for typical chorus, hiss, and EMIC waves.

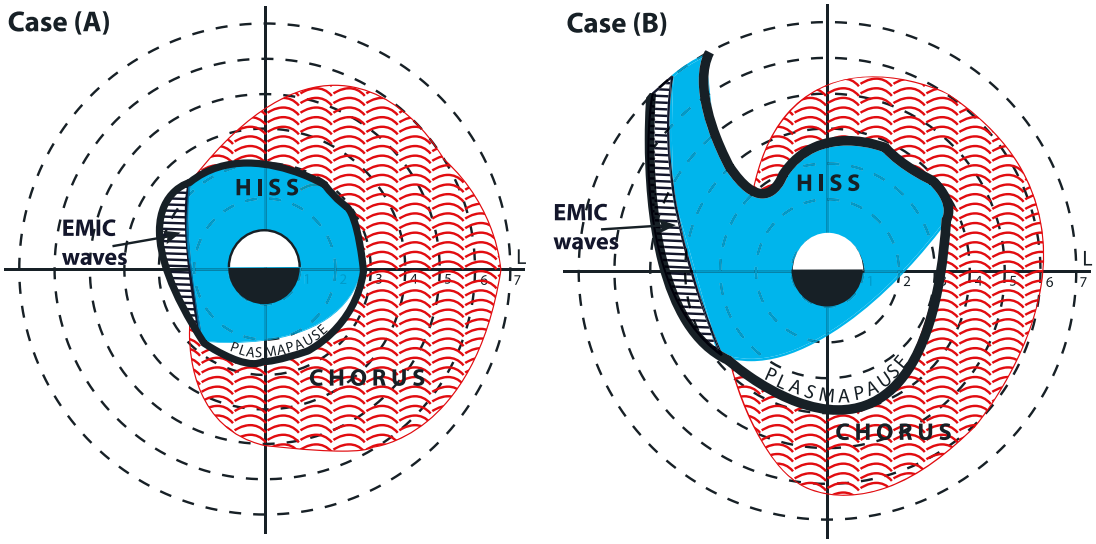

DRIFT-AVERAGE % FOR EACH WAVE MODE

	L = 3	4	5	6	7
chorus	63%	62%	47%	26%	0
hiss	14%	0	0	0	0
EMIC waves	9%	0	0	0	0

	L = 3	4	5	6	7
chorus	5%	68%	59%	32%	0
hiss	56%	11%	6%	4%	3%
EMIC waves	0	11%	4%	3%	2%

Figure 21. Schematic distributions of chorus, plasmaspheric hiss, and EMIC waves in the cases of high geomagnetic activity and relatively compressed plasmasphere (case A) and following high geomagnetic activity during the evolution of a plasmaspheric plume (case B). Corresponding to each case, a table is given showing the approximate percentage of an electron drift orbit that traverses each wave mode, for a given L value.

inside the plasmasphere or plume and $N_0 = 124\ (3/L)^4\ \mathrm{cm}^{-3}$ outside the plasmasphere. The results for the total electron loss timescale calculated from (1) and (2) are shown in the top of Figure 22. We also show in the bottom of Figure 22 the percentage contribution of each wave mode to the total electron loss rate, at the specified electron energies and L values. In both cases A and B, for electron energies 100 keV $\leq E_k \leq$ 1 MeV, we see that $\tau_{tot} \leq 1$ day, for $3 \leq L \leq 6$. For electrons in this energy range at these L values, the loss is the result of scattering by chorus or hiss or by chorus and hiss in combination. In case A, EMIC waves strongly scatter electrons of energy 3 MeV at $L = 3$. In case B, because of the presence of the plasmaspheric plume, EMIC waves produce intense scattering of 3 MeV electrons over the range $4 \leq L \leq 7$. Since the approximate minimum resonant energies for electron interaction with the assumed band of EMIC waves at $L = 3, 4, 5, 6, 7$ are $E_{\min} = 2.5, 2.1, 1.8, 1.5, 1.4$ MeV, respectively, EMIC waves cannot scatter electrons at the specified energies 100 keV, 300 keV, 1 MeV at $L = 3$ in case A or over the range $4 \leq L \leq 7$ in case B. At $L = 7$ scattering due to hiss in the plasmaspheric plume leads to approximate electron loss timescales of $\tau_{tot} = 3$ days for 300 keV electrons, and $\tau_{tot} = 20$ days for 1 MeV electrons. Cases A and B have been chosen to illustrate the differing contributions of each wave mode to the total scattering loss rate according to the state of the plasmasphere and the spatial distribution of the waves. To carry out more realistic calculations of the total electron loss timescale τ_{tot}, detailed information is required on the evolution over time of both the configuration of the plasmasphere and the wave distributions.

[34] We caution that the calculation of the total electron loss timescale by using (1) and (2) may be subject to limitations. Equations (1) and (2) assume that individual wave processes are additive and independent. This situation can at least be expected to prevail when diffusion is relatively weak. *Summers and Thorne* [2003] showed that EMIC waves can drive energetic electrons into the limit of strong diffusion, with a total precipitation loss of particles occurring in a few drift orbits. If total wave scattering is sufficiently intense to drive electrons into the strong diffusion regime, equations (1) and (2) become invalid. The electron loss timescale is then given by $\tau_{SD} = 1/D_{SD}$, where the strong diffusion rate D_{SD} is given by expression (27) of *Summers and Thorne* [2003].

[35] In this paper we have been concerned with loss of radiation belt electrons due to precipitation induced by plasma wave scattering. Net losses of radiation belt electrons may also result from radial (cross-L) diffusion and drift across the magnetospheric boundary (magnetopause shadowing). A comprehensive accounting of actual (non-adiabatic) losses of radiation belt electrons therefore

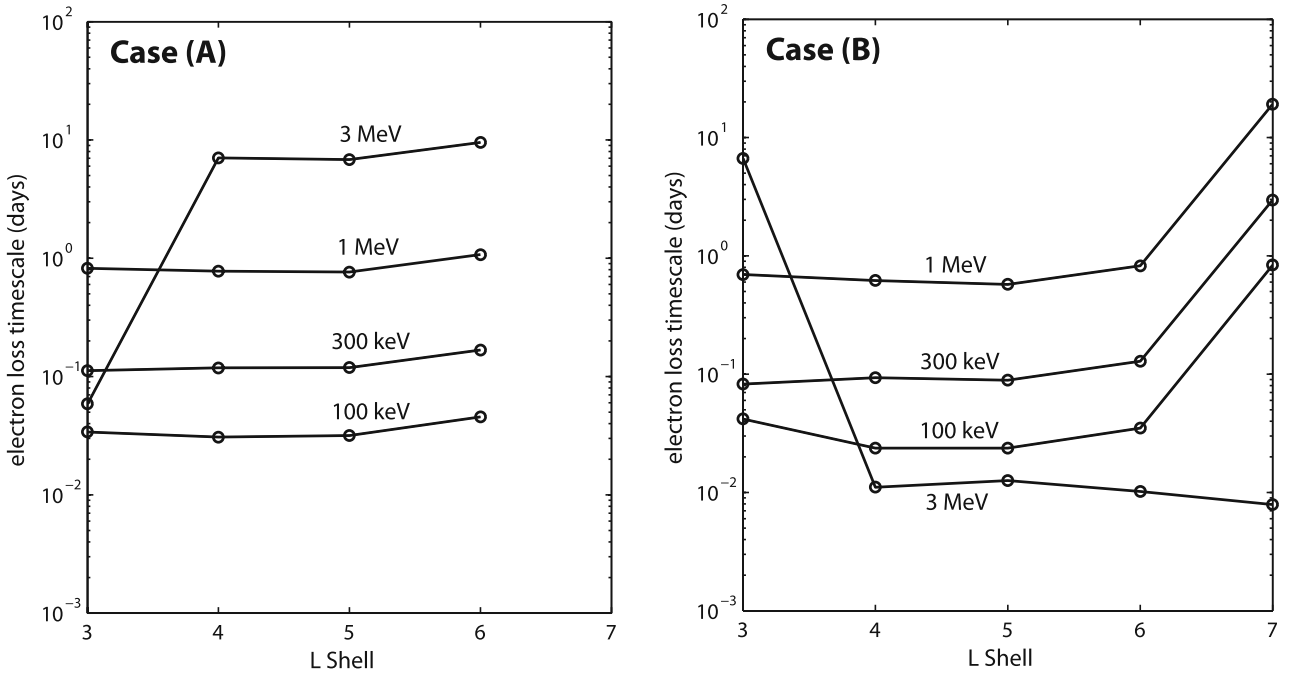

CONTRIBUTION OF EACH WAVE MODE TO TOTAL ELECTRON LOSS RATE

		L = 3	4	5	6	7
100keV	chorus	81%	100%	100%	100%	0
	hiss	19%	0	0	0	0
	EMIC	0	0	0	0	0
300keV	chorus	66%	100%	100%	100%	0
	hiss	34%	0	0	0	0
	EMIC	0	0	0	0	0
1MeV	chorus	71%	100%	100%	100%	0
	hiss	29%	0	0	0	0
	EMIC	0	0	0	0	0
3MeV	chorus	0.5%	100%	100%	100%	0
	hiss	0.2%	0	0	0	0
	EMIC	99.3%	0	0	0	0

		L = 3	4	5	6	7
100keV	chorus	7%	83%	93%	94%	0
	hiss	93%	17%	7%	6%	100%
	EMIC	0	0	0	0	0
300keV	chorus	4%	85%	93%	94%	0
	hiss	96%	15%	7%	6%	100%
	EMIC	0	0	0	0	0
1MeV	chorus	5%	86%	93%	94%	0
	hiss	95%	14%	7%	6%	100%
	EMIC	0	0	0	0	0
3MeV	chorus	5%	0.2%	0.2%	0.1%	0
	hiss	95%	0	0	0	0
	EMIC	0	99.8%	99.8%	99.9%	100%

Figure 22. Corresponding to Figure 21, total electron loss timescales due to combined scattering by chorus, plasmaspheric hiss, and EMIC waves in cases A and B. For each case, a table is given showing the approximate percentage contribution of each wave mode to the total electron loss rate.

requires inclusion of at least these additional processes. Evidence reported so far [e.g., *Reeves*, 2003] indicates that magnetopause shadowing does not cause significant electron losses from the outer zone.

6. Conclusions

[36] *Summers et al.* [2007] present formulae for the bounce-averaged quasi-linear diffusion coefficients for cyclotron resonance with field-aligned electromagnetic waves in a hydrogen or multi-ion (H^+, He^+, O^+) plasma. Here we have applied the formulae to the interaction of radiation belt electrons with (1) R-mode chorus waves outside the plasmasphere, (2) R-mode hiss inside the plasmasphere, and (3) L-mode EMIC waves inside the plasmasphere. Our main conclusions are as follows:

[37] 1. The process of bounce-averaging takes account of the off-equatorial resonant interactions of a particle with a wave during the bounce motion of the particle along the field line. For a given wave mode, the effects of bounce-averaging depend on the particle energy, equatorial pitch angle, L value, latitudinal distribution of the waves, and latitudinal distribution of plasma density. Bounce-averaging may increase, decrease, or leave unchanged the local pitch angle scattering rate at the equatorial loss cone. Compared to local equatorial values, bounce-averaging can increase the chorus momentum diffusion rates for energetic electrons, and extend the range of equatorial pitch angles over

which momentum diffusion is effective; bounce-averaging can also correspondingly reduce momentum diffusion rates at higher pitch angles for lower-energy electrons.

[38] 2. Timescales for momentum diffusion of MeV electrons in resonance with VLF chorus outside the plasmasphere can be optimally less than 1 day, or a few days, dependent on the properties of the waves, and the value of the parameter $\alpha^* = \Omega_e^2/\omega_{pe}^2 \propto B_0^2/N_0$. The mechanism of electron acceleration by chorus energy diffusion increases in efficiency as N_0 decreases or B_0 increases. Equatorial chorus waves ($|\lambda_W| < 15$ deg) can effectively accelerate MeV electrons of sufficiently large pitch angles; higher-latitude chorus ($|\lambda_W| > 15$ deg) increases the efficiency of the chorus acceleration mechanism. Timescales for precipitation loss of MeV electrons due to chorus scattering can be less than 1 day in the outer zone. Efficient pitch angle scattering of MeV electrons by field-aligned chorus typically requires waves with latitudinal distribution $|\lambda_W| > 30$ deg.

[39] 3. We have calculated timescales for the electron precipitation loss τ_{loss} due to pitch angle scattering by plasmaspheric hiss in the region $3 \leq L \leq 5$, during low geomagnetic activity ($K_p < 3^-$). For instance, at $L = 4$, we find $\tau_{loss} = 1.6$ days for electron energy $E_k = 510$ keV, and $\tau_{loss} = 6.1$ days for electron energy $E_k = 1.09$ MeV. We compared our model calculations with CRRES observations of timescales for the quiet-time decay of energetic electrons at $L = 3.0$, 3.5, 4.0, 4.5, and 5.0, following enhanced geomagnetic activity. For electron energies 510 keV $\leq E_k \leq 1$ MeV, the model timescales are a reasonable fit to the data, so we conclude that pitch angle scattering by field-aligned plasmaspheric hiss can largely account for the quiet-time decay of electrons at these energies in the region $3 \leq L \leq 5$. Timescales for electron precipitation loss due to hiss were found to be sensitive to the latitudinal distribution of the waves. We also calculated electron loss timescales due to hiss during high geomagnetic activity ($AE^* > 500$ nT) in the region $3 \leq L \leq 4$, using wave amplitudes measured on CRRES. Under these conditions, we found that plasmaspheric hiss can induce rapid precipitation loss of energetic electrons, e.g., at $L = 4$ we find $\tau_{loss} = 0.3$ day for $E_k = 510$ keV, and $\tau_{loss} = 1$ day for $E_k = 1.09$ MeV.

[40] 4. For EMIC waves, electron minimum resonant energies and pitch angle diffusion rates depend sensitively on the wave spectral properties, the ion (H^+, He^+, O^+) composition of the plasma, and the value of the parameter $\alpha^* = \Omega_e^2/\omega_{pe}^2$. Under appropriate conditions, hydrogen (H^+), helium (He^+), and oxygen (O^+) band EMIC waves, or EMIC waves in a hydrogen plasma, can induce precipitation loss of MeV electrons from the outer zone in a timescale of hours.

[41] 5. VLF chorus, plasmaspheric ELF hiss, and EMIC waves can each cause intense scattering loss of MeV electrons from the outer zone, under suitable conditions. Specifically, for each wave mode, the timescale for electron precipitation loss of MeV electrons can be of the order of hours or days. We conclude that scattering loss by chorus, hiss, or EMIC waves, can separately, or in combination, contribute significantly to the depletion of relativistic electrons from the outer radiation belt over the course of a magnetic storm. While chorus waves can efficiently accelerate electrons by energy diffusion (as noted in paragraph 2 above), plasmaspheric hiss and EMIC waves are not effective for electron acceleration.

[42] 6. To construct a complete model to describe the transport, acceleration and loss of radiation belt electrons, it is necessary to include, in addition to radial (cross-L) diffusion, resonant diffusion due to electron gyroresonance with VLF chorus, plasmaspheric ELF hiss, and EMIC waves. Accurate models of radiation belt electron dynamics require comprehensive observational data on the spectral properties of these waves, including not only the amplitudes and waveband parameters, but also the latitudinal and MLT distributions.

[43] **Acknowledgments.** This work is supported by the Natural Sciences and Engineering Research Council of Canada under grant A-0621.
[44] Zuyin Pu thanks Reiner Friedel and Sebastien Bourdarie for their assistance in evaluating this paper.

References

Albert, J. M. (1994), Quasi-linear pitch angle diffusion coefficients: Retaining high harmonics, *J. Geophys. Res.*, *99*, 23,741.
Albert, J. M. (2002), Nonlinear interaction of outer zone electrons with VLF waves, *Geophys. Res. Lett.*, *29*(8), 1275, doi:10.1029/2001GL013941.
Albert, J. M. (2003), Evaluation of quasi-linear diffusion coefficients for EMIC waves in a multispecies plasma, *J. Geophys. Res.*, *108*(A6), 1249, doi:10.1029/2002JA009792.
Anderson, R. R., and W. S. Kurth (1989), Discrete electromagnetic emissions in planetary magnetospheres, in *Plasma Waves and Instabilities at Comets and in Magnetospheres*, *Geophys. Monogr. Ser.*, vol. 53, edited by B. T. Tsurutani and H. Oya, p. 81, AGU, Washington, D. C.
Baker, D. N. (2002), How to cope with space weather, *Science*, *297*(5586), 1486.
Baker, D. N., et al. (1997), Recurrent geomagnetic storms and relativistic electron enhancements in the outer magnetosphere: ISTP coordinated measurements, *J. Geophys. Res.*, *102*, 14,141.
Baker, D. N., T. I. Pulkkinen, X. Li, S. G. Kanekal, J. B. Blake, R. S. Selesnick, M. G. Henderson, G. D. Reeves, H. E. Spence, and G. Rostoker (1998), Coronal mass ejections, magnetic clouds, and relativistic magnetospheric electron events: ISTP, *J. Geophys. Res.*, *103*, 17,279.
Blake, J. B., D. N. Baker, N. Turner, K. W. Ogilvie, and R. P. Lepping (1997), Correlation of changes in the outer-zone relativistic-electron population with upstream solar wind and magnetic field measurements, *Geophys. Res. Lett.*, *24*, 927.
Bortnik, J., U. S. Inan, and T. F. Bell (2006), Landau damping and resultant unidirectional propagation of chorus waves, *Geophys. Res. Lett.*, *33*, L03102, doi:10.1029/2005GL024553.
Bräysy, T., K. Mursula, and G. Marklund (1998), Ion cyclotron waves during a great magnetic storm observed by Freja double-probe electric field instrument, *J. Geophys. Res.*, *103*, 4145.
Burch, J. L. (2006), New insights on magnetospheric processes from IMAGE, paper presented at Conference on Earth-Sun System Exploration: Energy Transfer, Johns Hopkins Univ. Appl. Phys. Lab., Kona, Hawaii.
Burch, J. L., W. S. Lewis, T. J. Immel, P. C. Anderson, H. U. Frey, S. A. Fuselier, J. C. Gerard, S. B. Mende, D. G. Mitchell, and M. F. Thomsen (2002), Interplanetary magnetic field control of afternoon-sector detached proton auroral arcs, *J. Geophys. Res.*, *107*(A9), 1251, doi:10.1029/2001JA007554.
Burtis, W. J., and R. A. Helliwell (1975), Magnetospheric chorus: Amplitude and growth rate, *J. Geophys. Res.*, *80*, 3265.
Burtis, W. J., and R. A. Helliwell (1976), Magnetospheric chorus: Occurrence patterns and normalized frequency, *Planet. Space Sci.*, *24*, 1007.
Church, S. R., and R. M. Thorne (1983), On the origin of plasmaspheric hiss: Ray path integrated amplification, *J. Geophys. Res.*, *88*, 7941.
Clilverd, M. A., C. J. Rodger, and T. Ulick (2006), The importance of atmospheric precipitation in storm-time relativistic electron flux dropouts, *Geophys. Res. Lett.*, *33*, L01102, doi:10.1029/2005GL024661.
Cornilleau-Wehrlin, N., J. Solomon, A. Korth, and G. Kremser (1993), Generation mechanism of plasmaspheric ELF/VLF hiss: A statistical study from GEOS 1 data, *J. Geophys. Res.*, *98*, 21,471.
Elkington, S. R., M. K. Hudson, and A. A. Chan (2003), Resonant acceleration and diffusion of outer zone electrons in an asymmetric geomagnetic field, *J. Geophys. Res.*, *108*(A3), 1116, doi:10.1029/2001JA009202.
Erlandson, R. E., and A. J. Ukhorskiy (2001), Observations of electromagnetic ion cyclotron waves during geomagnetic storms: Wave occurrence and pitch angle scattering, *J. Geophys. Res.*, *106*, 3883.

Fraser, B. J., and T. S. Nguyen (2001), Is the plasmapause a preferred source region of electromagnetic ion cyclotron waves in the magnetosphere?, *J. Atmos. Sol. Terr. Phys.*, *63*, 1225.

Fraser, B. J., H. J. Singer, W. J. Hughes, J. R. Wygant, R. R. Anderson, and Y. D. Hu (1996), CRRES Poynting vector observations of electromagnetic ion cyclotron waves near the plasmapause, *J. Geophys. Res.*, *101*, 15,331.

Friedel, R. H. W., G. D. Reeves, and T. Obara (2002), Relativistic electron dynamics in the inner magnetosphere - A review, *J. Atmos. Sol. Terr. Phys.*, *64*, 265.

Gendrin, R. (2001), The role of wave particle interactions in radiation belts modeling, in *Sun-Earth Connection and Space Weather*, Vol. 75, edited by M. Candidi, M. Storini, and U. Villante, p. 151, SIF, Bologna.

Glauert, S. A., and R. B. Horne (2005), Calculation of pitch angle and energy diffusion coefficients with the PADIE code, *J. Geophys. Res.*, *110*, A04206, doi:10.1029/2004JA010851.

Goldstein, J., B. R. Sandel, M. F. Thomsen, M. Spasojevic, and P. H. Reiff (2004), Simultaneous remote sensing and in situ observations of plasmaspheric drainage plumes, *J. Geophys. Res.*, *109*, A03202, doi:10.1029/2003JA010281.

Goldstein, J., B. R. Sandel, W. T. Forrester, M. F. Thomsen, and M. R. Hairston (2005), Global plasmasphere evolution 22–23 April 2001, *J. Geophys. Res.*, *110*, A12218, doi:10.1029/2005JA011282.

Green, J. C., and M. G. Kivelson (2004), Relativistic electrons in the outer radiation belt: Differentiating between acceleration mechanisms, *J. Geophys. Res.*, *109*, A03213, doi:10.1029/2003JA010153.

Green, J. C., T. G. Onsager, T. P. O'Brien, and D. N. Baker (2004), Testing loss mechanisms capable of rapidly depleting relativistic electron flux in the Earth's outer radiation belt, *J. Geophys. Res.*, *109*, A12211, doi:10.1029/2004JA010579.

Green, J. C., T. P. O'Brien, T. G. Onsager, B. J. Fraser, H. J. Singer, S. G. Kanekal, D. N. Baker, and R. F. Friedel (2005), A review of the processes which deplete radiation belt electron flux, paper presented at Workshop on Energetic Electron Radiation Belt Dynamics, Hermanus Magn. Obs., Hermanus, South Africa.

Hayakawa, M., and S. S. Sazhin (1992), Mid-latitude and plasmaspheric hiss: A review, *Planet. Space Sci.*, *40*, 1325.

Horne, R. B. (2002), The contribution of wave-particle interactions to electron loss and acceleration in the Earth's radiation belts during geomagnetic storms, in *Review of Radio Science 1999–2002*, edited by W. R. Stone, chap. 33, pp. 801–828, John Wiley, Hoboken, N. J.

Horne, R. B., R. M. Thorne, S. A. Glauert, J. M. Albert, N. P. Meredith, and R. R. Anderson (2005a), Timescale for radiation belt electron acceleration by whistler mode chorus waves, *J. Geophys. Res.*, *110*, A03225, doi:10.1029/2004JA010811.

Horne, R. B., et al. (2005b), Wave acceleration of electrons in the Van Allen radiation belts, *Nature*, *437*, 227, doi:10.1038/nature03939.

Hudson, M. K., S. R. Elkington, J. G. Lyon, M. J. Wiltberger, and M. Lessard (2001), Radiation belt electron acceleration by ULF wave drift resonance: Simulation of 1997 and 1998 storms, in *Space Weather*, *Geophys. Monogr. Ser.*, vol. 125, edited by P. Song, H. J. Singer, and G. L. Siscoe, p. 289, AGU, Washington, D. C.

Iles, R. H. A., N. P. Meredith, A. N. Fazakerley, and R. B. Horne (2006), Phase space density analysis of the outer radiation belt energetic electron dynamics, *J. Geophys. Res.*, *111*, A03204, doi:10.1029/2005JA011206.

Jordanova, V. K., C. J. Farrugia, R. M. Thorne, G. V. Khazanov, G. D. Reeves, and M. F. Thomsen (2001), Modeling ring current proton precipitation by electromagnetic ion cyclotron waves during the May 14–16, 1997, storm, *J. Geophys. Res.*, *106*, 7.

Katoh, Y., and Y. Omura (2004), Acceleration of relativistic electrons due to resonant scattering by whistler mode waves generated by temperature anisotropy in the inner magnetosphere, *J. Geophys. Res.*, *109*, A12214, doi:10.1029/2004JA010654.

Kennel, C. F., and H. E. Petschek (1966), Limit on stably trapped particle fluxes, *J. Geophys. Res.*, *71*, 1.

Kim, H.-J., and A. A. Chan (1997), Fully adiabatic changes in storm-time relativistic electron fluxes, *J. Geophys. Res.*, *102*, 22,107.

Koons, H. C., and J. L. Roeder (1990), A survey of equatorial magnetospheric wave activity between 5 and 8 R_E, *Planet. Space Sci.*, *38*, 1335.

Li, X., and M. A. Temerin (2001), The electron radiation belt, *Space Sci. Rev.*, *95*, 569.

Li, X., I. Roth, M. A. Temerin, J. R. Wygant, M. K. Hudson, and J. B. Blake (1993), Simulation of the prompt energization and transport of radiation belt particles during the March 24, 1991 SSC, *Geophys. Res. Lett.*, *20*, 2324.

Li, X., D. N. Baker, M. A. Temerin, T. E. Cayton, E. G. D. Reeves, R. A. Christensen, J. B. Blake, M. D. Looper, R. Nakamura, and S. G. Kanekal (1997), Multi-satellite observations of the outer zone electron variation during the November 3–4, 1993, magnetic storm, *J. Geophys. Res.*, *102*, 14,123.

Lorentzen, K. R., M. P. McCarthy, G. K. Parks, J. E. Foat, R. M. Millan, D. M. Smith, R. P. Lin, and J. P. Treilhou (2000), Precipitation of relativistic electrons by interaction with electromagnetic ion cyclotron waves, *J. Geophys. Res.*, *105*, 5381.

Lorentzen, K. R., J. B. Blake, U. S. Inan, and J. Bortnik (2001), Observations of relativistic electron microbursts in association with VLF chorus, *J. Geophys. Res.*, *106*, 6017.

Loto'aniu, T. M., R. M. Thorne, B. J. Fraser, and D. Summers (2006), Estimating relativistic electron pitch angle scattering rates using properties of the electromagnetic ion cyclotron wave spectrum, *J. Geophys. Res.*, *111*, A04220, doi:10.1029/2005JA011452.

Lyons, L. R., R. M. Thorne, and C. F. Kennel (1972), Pitch-angle diffusion of radiation belt electrons within the plasmasphere, *J. Geophys. Res.*, *77*, 3455.

Masson, A., U. S. Inan, H. Laakso, O. Santolik, and P. Decreau (2004), Cluster observations of mid-latitude hiss near the plasmapause, *Ann. Geophys.*, *22*, 2565.

Meredith, N. P., R. B. Horne, and R. R. Anderson (2001), Substorm dependence of chorus amplitudes: Implications for the acceleration of electrons to relativistic energies, *J. Geophys. Res.*, *106*, 13,165.

Meredith, N. P., R. B. Horne, R. H. A. Iles, R. M. Thorne, D. Heynderickx, and R. R. Anderson (2002a), Outer zone relativistic electron acceleration associated with substorm-enhanced whistler mode chorus, *J. Geophys. Res.*, *107*(A7), 1144, doi:10.1029/2001JA900146.

Meredith, N. P., R. B. Horne, D. Summers, R. M. Thorne, R. H. A. Iles, D. Heynderickx, and R. R. Anderson (2002b), Evidence for acceleration of outer zone electrons to relativistic energies by whistler mode chorus, *Ann. Geophys.*, *20*, 967.

Meredith, N. P., R. B. Horne, R. M. Thorne, and R. R. Anderson (2003a), Favored regions for chorus-driven electron acceleration to relativistic energies in the Earth's outer radiation belt, *Geophys. Res. Lett.*, *30*(16), 1871, doi:10.1029/2003GL017698.

Meredith, N. P., M. Cain, R. B. Horne, R. M. Thorne, D. Summers, and R. R. Anderson (2003b), Evidence for chorus-driven electron acceleration to relativistic energies from a survey of geomagnetically disturbed periods, *J. Geophys. Res.*, *108*(A6), 1248, doi:10.1029/2002JA009764.

Meredith, N. P., R. M. Thorne, R. B. Horne, D. Summers, B. J. Fraser, and R. R. Anderson (2003c), Statistical analysis of relativistic electron energies for cyclotron resonance with EMIC waves observed on CRRES, *J. Geophys. Res.*, *108*(A6), 1250, doi:10.1029/2002JA009700.

Meredith, N. P., R. B. Horne, R. M. Thorne, D. Summers, and R. R. Anderson (2004), Substorm dependence of plasmaspheric hiss, *J. Geophys. Res.*, *109*, A06209, doi:10.1029/2004JA010387.

Meredith, N. P., R. B. Horne, S. A. Glauert, R. M. Thorne, D. Summers, J. M. Albert, and R. R. Anderson (2006), Energetic outer zone electron loss timescales during low geomagnetic activity, *J. Geophys. Res.*, *111*, A05212, doi:10.1029/2005JA011516.

Millan, R. M., R. P. Lin, D. M. Smith, K. R. Lorentzen, and M. P. McCarthy (2002), X-ray observations of MeV electron precipitation with a balloon-borne germanium spectrometer, *Geophys. Res. Lett.*, *29*(24), 2194, doi:10.1029/2002GL015922.

Miyoshi, Y., A. Morioka, T. Obara, H. Misawa, T. Nagai, and Y. Kasahara (2003), Rebuilding process of the outer radiation belt during the 3 November 1993 magnetic storm: NOAA and Exos-D observations, *J. Geophys. Res.*, *108*(A1), 1004, doi:10.1029/2001JA007542.

Moldwin, M. B., J. Howard, J. Sanny, J. D. Bocchicchio, H. K. Rassoul, and R. R. Anderson (2004), Plasmaspheric plumes: CRRES observations of enhanced density beyond the plasmapause, *J. Geophys. Res.*, *109*, A05202, doi:10.1029/2003JA010320.

O'Brien, T. P., K. R. Lorentzen, I. R. Mann, N. P. Meredith, J. B. Blake, J. F. Fennell, M. D. Looper, D. K. Milling, and R. R. Anderson (2003), Energization of relativistic electrons in the presence of ULF power and MeV microbursts: Evidence for dual ULF and VLF acceleration, *J. Geophys. Res.*, *108*(A8), 1329, doi:10.1029/2002JA009784.

O'Brien, T. P., M. D. Looper, and J. B. Blake (2004), Quantification of relativistic electron microburst losses during the GEM storms, *Geophys. Res. Lett.*, *31*, L04802, doi:10.1029/2003GL018621.

Omura, Y., and D. Summers (2006), Dynamics of high-energy electrons interacting with whistler mode chorus emissions in the magnetosphere, *J. Geophys. Res.*, *111*, A09222, doi:10.1029/2006JA011600.

Onsager, T. G., G. Rostoker, H. Kim, G. D. Reeves, T. Obara, H. J. Singer, and C. Smithtro (2002), Radiation belt electron flux dropouts: Local time, radial, and particle-energy dependence, *J. Geophys. Res.*, *107*(A11), 1382, doi:10.1029/2001JA000187.

Parrot, M., and C. A. Gaye (1994), A statistical survey of ELF waves in a geostationary orbit, *Geophys. Res. Lett.*, *21*, 2463.

Parrot, M., and F. Lefeuvre (1986), Statistical study of the propagation characteristics of ELF hiss observed on GEOS-1, inside and outside the plasmasphere, *Ann. Geophys.*, *4*, 363.

Reeves, G. D. (2003), The life history of a "killer": The origin and fate of relativistic electrons, paper presented at 2003 General Assembly, Int. Union of Geod. and Geophys., Sapporo, Japan.

Reeves, G. D., D. N. Baker, R. D. Belian, J. B. Blake, T. E. Cayton, J. F. Fennell, R. H. W. Friedel, M. M. Meier, R. S. Selesnick, and H. E. Spence (1998), The global response of relativistic radiation belt electrons to the January 1997 magnetic cloud, *Geophys. Res. Lett.*, *25*, 3265.

Reeves, G. D., K. L. McAdams, R. H. W. Friedel, and T. P. O'Brien (2003), Acceleration and loss of relativistic electrons during geomagnetic storms, *Geophys. Res. Lett.*, *30*(10), 1529, doi:10.1029/2002GL016513.

Roth, I., M. Temerin, and M. K. Hudson (1999), Resonant enhancement of relativistic electron fluxes during geomagnetically active periods, *Ann. Geophys.*, *17*, 631.

Santolik, O., D. A. Gurnett, J. S. Pickett, M. Parrot, and N. Cornilleau-Wehrlin (2003), Spatio-temporal structure of storm-time chorus, *J. Geophys. Res.*, *108*(A7), 1278, doi:10.1029/2002JA009791.

Santolik, O., D. A. Gurnett, J. S. Pickett, M. Parrot, and N. Cornilleau-Wehrlin (2004), A microscopic and nanoscopic view of storm-time chorus on 31 March 2001, *Geophys. Res. Lett.*, *31*, L02801, doi:10.1029/2003GL018757.

Santolik, O., E. Macusova, K. H. Yearby, N. Cornilleau-Wehrlin, and H. S. K. Alleyne (2005), Radial variation of whistler-mode chorus: First results from the STAFF/DWP instrument on board the Double Star TC-1 spacecraft, *Ann. Geophys.*, *23*, 2937.

Sazhin, S. S., and M. Hayakawa (1992), Magnetospheric chorus emissions: A review, *Planet. Space Sci.*, *40*, 681.

Schulz, M., and L. Lanzerotti (1974), *Particle Diffusion in the Radiation Belts*, Springer, New York.

Sheeley, B. W., M. B. Moldwin, H. K. Rassoul, and R. R. Anderson (2001), An empirical plasmasphere and trough density model: CRRES observations, *J. Geophys. Res.*, *106*, 25,631.

Shprits, Y. Y., R. M. Thorne, R. B. Horne, S. A. Glauert, M. Cartwright, C. T. Russell, D. N. Baker, and S. G. Kanekal (2006a), Acceleration mechanism responsible for the formation of the new radiation belt during the 2003 Halloween solar storm, *Geophys. Res. Lett.*, *33*, L05104, doi:10.1029/2005GL024256.

Shprits, Y. Y., R. M. Thorne, R. B. Horne, and D. Summers (2006b), Bounce-averaged diffusion coefficients for field-aligned chorus waves, *J. Geophys. Res.*, *111*, A10225, doi:10.1029/2006JA011725.

Smith, A. J., N. P. Meredith, and T. P. O'Brien (2004), Differences in ground-observed chorus in geomagnetic storms with and without enhanced relativistic electron fluxes, *J. Geophys. Res.*, *109*, A11204, doi:10.1029/2004JA010491.

Smith, E. J., A. M. A. Frandsen, B. T. Tsurutani, R. M. Thorne, and K. W. Chan (1974), Plasmaspheric hiss intensity variations during magnetic storms, *J. Geophys. Res.*, *79*, 2507.

Solomon, J., N. Cornilleau-Wehrlin, A. Korth, and G. Kremser (1988), An experimental study of ELF/VLF hiss generation in the Earth's magnetosphere, *J. Geophys. Res.*, *93*, 1839.

Spasojevic, M., J. Goldstein, D. L. Carpenter, U. S. Inan, B. R. Sandel, M. B. Moldwin, and B. W. Reinisch (2003), Global response of the plasmasphere to a geomagnetic disturbance, *J. Geophys. Res.*, *108*(A9), 1340, doi:10.1029/2003JA009987.

Spasojevic, M., H. U. Frey, M. F. Thomsen, S. A. Fuselier, S. P. Gary, B. R. Sandel, and U. S. Inan (2004), The link between a detached subauroral proton arc and a plasmaspheric plume, *Geophys. Res. Lett.*, *31*, L04803, doi:10.1029/2003GL018389.

Summers, D. (2005), Quasi-linear diffusion coefficients for field-aligned electromagnetic waves with applications to the magnetosphere, *J. Geophys. Res.*, *110*, A08213, doi:10.1029/2005JA011159.

Summers, D., and C. Ma (2000), A model for generating relativistic electrons in the Earth's inner magnetosphere based on gyroresonant wave-particle interactions, *J. Geophys. Res.*, *105*, 2625.

Summers, D., and R. M. Thorne (2003), Relativistic electron pitch angle scattering by electromagnetic ion cyclotron waves during geomagnetic storms, *J. Geophys. Res.*, *108*(A4), 1143, doi:10.1029/2002JA009489.

Summers, D., R. M. Thorne, and F. Xiao (1998), Relativistic theory of wave-particle resonant diffusion with application to electron acceleration in the magnetosphere, *J. Geophys. Res.*, *103*, 20,487.

Summers, D., C. Ma, N. P. Meredith, R. B. Horne, R. M. Thorne, D. Heynderickx, and R. R. Anderson (2002), Model of the energization of outer-zone electrons by whistler-mode chorus during the October 9, 1990 geomagnetic storm, *Geophys. Res. Lett.*, *29*(4), 2174, doi:10.1029/2002GL016039.

Summers, D., C. Ma, and T. Mukai (2004a), Competition between acceleration and loss mechanisms of relativistic electrons during geomagnetic storms, *J. Geophys. Res.*, *109*, A04221, doi:10.1029/2004JA010437.

Summers, D., C. Ma, N. P. Meredith, R. B. Horne, R. M. Thorne, and R. R. Anderson (2004b), Modeling outer-zone relativistic electron response to whistler-mode chorus activity during substorms, *J. Atmos. Sol. Terr. Phys.*, *66*, 133.

Summers, D., R. L. Mace, and M. A. Hellberg (2005), Pitch-angle scattering rates in planetary magnetospheres, *J. Plasma Phys.*, *71*(3), 237.

Summers, D., B. Ni, and N. P. Meredith (2007), Timescales for radiation belt electron acceleration and loss due to resonant wave-particle interactions: 1. Theory, *J. Geophys. Res.*, *112*, A04206, doi:10.1029/2006JA011801.

Thorne, R. M., E. J. Smith, K. J. Fiske, and S. R. Church (1974), Intensity variation of ELF hiss and chorus during isolated substorms, *Geophys. Res. Lett.*, *1*, 193.

Thorne, R. M., R. B. Horne, S. A. Glauert, N. P. Meredith, Y. Shprits, D. Summers, and R. R. Anderson (2005a), The influence of wave-particle interactions on relativistic electron dynamics during storms, in *Inner Magnetosphere Interactions: New Perspectives From Imaging*, *Geophys. Monogr. Ser.*, vol. 159, edited by J. Burch, M. Schulz, and H. Spence, p. 101, AGU, Washington, D. C.

Thorne, R. M., T. P. O'Brien, Y. Y. Shprits, D. Summers, and R. B. Horne (2005b), Timescale for MeV electron microburst loss during geomagnetic storms, *J. Geophys. Res.*, *110*, A09202, doi:10.1029/2004JA010882.

Trakhtengerts, V. Y., M. J. Rycroft, D. Nunn, and A. G. Demekhov (2003), Cyclotron acceleration of radiation belt electrons by whistlers, *J. Geophys. Res.*, *108*(A3), 1138, doi:10.1029/2002JA009559.

Tsurutani, B. T., and E. J. Smith (1974), Postmidnight chorus: A substorm phenomenon, *J. Geophys. Res.*, *79*, 118.

Tsurutani, B. T., and E. J. Smith (1977), Two types of magnetospheric ELF chorus and their substorm dependences, *J. Geophys. Res.*, *82*, 5112.

Tsurutani, B. T., E. J. Smith, and R. M. Thorne (1975), Electromagnetic hiss and relativistic electron losses in the inner zone, *J. Geophys. Res.*, *80*, 600.

Varotsou, A., D. Boscher, S. Bourdarie, R. B. Horne, S. A. Glauert, and N. P. Meredith (2005), Simulation of the outer radiation belt electrons near geosynchronous orbit including both radial diffusion and resonant interaction with whistler-mode chorus waves, *Geophys. Res. Lett.*, *32*, L19106, doi:10.1029/2005GL023282.

N. P. Meredith, British Antarctic Survey, Natural Environment Research Council, Madingley Road, Cambridge, CB3 0ET, UK. (nmer@bas.ac.uk)

B. Ni and D. Summers, Department of Mathematics and Statistics, Memorial University of Newfoundland, St. John's, Newfoundland, Canada A1C 5S7. (bbni@math.mun.ca; dsummers@math.mun.ca)